報告番号 甲第 4014 号

Molecular Mechanism of Bubble Formation in Liquids

Tomoyuki Kinjo

Molecular Mechanism of Bubble Formation in Liquids

Tomoyuki Kinjo
Depertment of Applied Physics, School of Engineering
Nagoya University, Nagoya, 464-01, Japan

1998

ABSTRACT

Molecular dynamics simulations were carried out to investigate the molecular mechanism of bubble formation in unary and binary liquids. In the simulations of unary liquid, the system consists of 10,976 particles which interact each other via the Lennard-Jones potential. The stability limits of liquid were obtained. It is found that bubble growth has two stages, growth-shrinkage, and explosive growth. The nucleation rate calculated from the waiting time for bubble formation is 17 orders of magnitude larger than prediction of classical nucleation theory. In the simulations of binary liquid, the system consists of 960 solute molecules and 10,016 solvent molecules which interact each other via the Lennard-Jones potential with Lorentz-Bertherot mixing rule. It is found that bubble formation and growth are associated with clustering of solute molecules. The total surface adsorption is also calculated.

A part of this work was presented by the author at

- ICCT-96,Osaka, Japan, Aug. 1996
- ICHMT symposium, Yokohama, Japan, Dec. 1996
- International Symposium on Molecular Thermodynamics and Molecular Simulation, Tokyo, Japan, Jan. 1997
- IUMRS-ICA-97, Chiba, Japan, Sept. 1997
- American Institute of Chemical Engineers 1997 Annual Meeting, Los Angeles, USA, Nov. 1997

ACKNOWLEDGMENTS

I would like to thank Prof. Mitsuhiro Matsumoto, Depertment of Applied Physics, School of Engineering, Nagoya University, for helpful suggestions and comments. I also would like to thank Prof. Masao Doi, Nagoya University, for stimulating discussion.

I wish to express my gratitude to Dr.R. Yamamoto, Kyoto University, for helpful suggestion on several points of calculation. Thanks are also due to Dr. K. Yasuoka, RIKEN, Dr. T. Taniguchi, Nagoya University Dr. T. Okuzono Nagoya University, for helpful discussion.

I wold like to thank Dr. Yamada and other member of our laboratory.

A part of the calculation was carried out at the Institute of Solid State Physics, University of Tokyo.

My special thanks are due to my parents for continuing encouragement.

Tomoyuki Kinjo

Nagoya, Junuary 23, 1998

Contents

Chapter 1

INTRODUCTION

Bubble formation in liquids is of considerable technical importance and scientific interest [1].

In several industrial processes, two liquid having different temperatures come into contact. When the colder liquid is more volatile than the hotter one, the former can vaporize suddenly and explosively. This is called "vapor explosion", which often causes a disastrous phenomena, such as coolant explosion in a melt-down accident of atomic reactors or vapor explosion in volcano areas. To avoid them, the prediction of conditions under which liquids can undergo explosive boiling is important.

In physics, dynamics of first-order phase transition has long been of great interest as a fundamental subject of statistical physics [2, 3]. Theoretical treatment is usually based on a so-called classical nucleation theory [4], but its reliability can be questionable near the spinodal region. The subject of this thesis, bubble formation, is a typical example of such nucleation phenom-

ena. Bubbles are generated by another way. For example, ultrasonic waves irradiated to liquids generate high frequency pressure oscillation and form microscale cavities. The gas in the oscillating cavity becomes extremely hot and begins to emit light of broad spectrum, which is called sonoluminescence. Its molecular mechanism in detail is not fully understood yet.

Bubble formation is also important in botany [1]. For trees, columns of sap transport water from their roots under the ground to their top. When the tree is very tall, the pressure at the top of sap columns can be negative. The water transportation is possible only when the water is in a metastable liquid state under such pressure; otherwise, formed bubbles prevent the transportation.

Cavitation takes an important role also in medicine, such as decompression sickness (bubble formation in blood by sudden pressure decrease) and cracking of joints.

Thus, bubble formation is observed in various fields. Its mechanism, however, has long been studied mainly from macroscopic (eg., thermodynamic and hydrodynamic) points of view. In recent years, understanding of bubble formation in liquids at microscopic level is required in many fields, because rapid phase change in extreme conditions becomes more and more important associating with various technology advancements. However, experiments (microscopic observation) and rigorous theoretical treatments still have many difficulties at this stage.

Computer simulation provides a useful tool to explore these microscale dynamics. In particular, molecular dynamics (MD) simulation [5], which is a method to solve a set of equations of motion for each molecule and to pursue its trajectory, has gradually become popular in many fields. It requires large amount of computer resource to simulate many particle system for a long period, but recent advancement in hardware enables us to apply this method to study various phenomena.

In this thesis, I adopt the MD method to explore the microscopic dynamics of bubble formation. This kind of simulation has been very difficult until recently because large system size is necessary to treat hydrodynamic effects properly.

The thesis consists of four chapters.

In Chapter 1, I describe theoretical and experimental backgrounds. Classical nucleation theory is reviewed in some detail since its applicability in extreme nonequilibrium conditions is one of the main topics.

Chapters 2 and 3 are the main part of this thesis. In Chapter 2, I study the homogeneous bubble formation (cavitation) in unary liquid under negative pressure. Chapter 3 is devoted to the study of degassing process in binary (solvent with gaseous solute) liquid system. Phase change from metastable liquid to vapor via bubble formation is observed in both process, but it is found that their microscopic mechanism is quite different.

The main results are summarized in Chapter 4.

1.1 The Thermodynamic Limit

The first order phase transition is the transition from a metastable state to a stable state. Metastable states are the states which is stable against small fluctuations but its free energy is not globally minimum. This metastable region in a phase diagram has a boundary beyond which the state is not stable against even an infinitesimal perturbation. This boundary is called the "thermodynamic limit" or the spinodal line. In this section, I describe the definition and some properties of the thermodynamic limit of stability.

Thermodynamic systems can be categorized as either being stable, metastable or unstable in terms of free energy. The global minimum corresponds to the stable state, while the free energy of metastable states is locally minimum but not a global minimum. All other states are unstable. From the viewpoint of stability against small fluctuations, both stable and metastable states show similar behavior; in the following part, we refer both states as a "stable" state.

Now, let us consider the thermodynamic limits for n-compornent systems.

If an isolated system is in equilibrium, the change of the system's entropy for any processes which satisfy the isolation conditions must be

$$(\Delta S)_{U,V,N} \leq 0 \tag{1.1}$$

There are several inequalities equivalent to the above:

$$(\Delta U)_{S,V,N} \geq 0 \tag{1.2}$$

$$(\Delta F)_{T,V,N} \geq 0 \tag{1.3}$$

$$(\Delta G)_{T,P,N} \geq 0 \tag{1.4}$$

Let us consider the equation(1.2). ΔU can be expanded in Taylor series as,

$$(\Delta U)_{S,V,N} = \left(\delta U + \frac{1}{2}\delta^2 U + \cdots\right)_{S,V,N} \geq 0. \tag{1.5}$$

For the equilibrium conditions,

$$\delta U = 0. \tag{1.6}$$

Also, for the equilibrium state to be stable, we require

$$\delta^2 U > 0. \tag{1.7}$$

The condition of violation of the equation(1.7) determines the limit of stability.

For $n-$compornent fluids, we can write

$$\begin{aligned} \delta U &= T\delta S - P\delta V + \sum_{j=1}^{n} \mu_j \delta N_j \\ &\equiv \sum_{j=1}^{n+2} \xi_j \delta X_j, \end{aligned} \tag{1.8}$$

where $\{X_i\}$ represents extensive parameters (S,V, and $N_1,\cdots,N_n$), and $\{\xi_i\}$ the conjugate intensive parameters. Consider an isolated system of given S,V and N_i at equilibrium. By dividing the system into two subsystems, we can transform the equation(1.7) to the quadratic form [6]:

$$\sum_{i=1}^{n+2}\sum_{j=1}^{n+2} A_{ij}\delta X_i' \delta X_j' > 0, \tag{1.9}$$

where A_{ij} is a linear combination of second derivatives of U, or $\partial\xi_i/\partial X_j$. This leads to the inequality,

$$\left(\frac{\partial \xi_{n+1}}{\partial X_{n+1}}\right)_{\xi_1,\cdots,\xi_n,X_{n+2}} > 0 \tag{1.10}$$

At a thermodynamic limit, we have

$$\left(\frac{\partial \xi_{n+1}}{\partial X_{n+1}}\right)_{\xi_1,\cdots,\xi_n,X_{n+2}} = 0. \tag{1.11}$$

For pure fluids ($n = 1$), ξ_i ($i = 1, 2, 3$) can be either T, $-p$, or μ. Then, X_i is either S, V, or N, respectively. In this case, (1.10) is a condition about a second derivative of a variable. Therefore 6 inequalities can be obtained. The following two expressions are particularly useful:

$$\left(\frac{\partial T}{\partial S}\right)_{p,N} > 0 \quad \text{or} \quad \left(\frac{\partial T}{\partial s}\right)_{p} = \frac{T}{c_p} > 0, \tag{1.12}$$

$$-\left(\frac{\partial p}{\partial V}\right)_{T,N} > 0 \quad \text{or} \quad -\left(\frac{\partial p}{\partial v}\right)_{T} = \frac{1}{v\kappa_T} > 0, \tag{1.13}$$

where s and v are entropy per molecule or volume per molecule. (1.12) implies that if heat is added to a stable(or metastable) state at constant pressure, the system temperature must rise(thermal criterion). (1.13) implies that if the system is compressed isothermally, its pressure must increase(mechanical criterion).

The limit conditions (1.11) are satisfied simultaneously on a phase point; in other words, the stability conditions (1.10) are broken simultaneously.

1.2 Classical Nucleation Theory

When a metastable phase undergoes phase transition in absence of impurities or solid boundaries, nuclei of the stable phase must be formed in the bulk metastable phase. This process is known as homogeneous nucleation.

In this section, I briefly describe the classical nucleation theory originally developed by Becker and Döring [7]. The theory aims at calculating the net rate J at which nuclei grow to the critical size beyond which the new phase forms spontaneously.

1.2.1 Nucleation in supersaturated vapors

First, we consider cluster(of liquid drop) formation in supersaturated (or supercooled) vapors. Extension to bubble formation in superheated liquids will be discussed in the next section.

Suppose that clusters change their size only by single-molecule (step-by-step) events. Then a flux $J(n)$, the net rate at which size-$(n-1)$ clusters become size-n, can be written as

$$J(n) = f(n-1)A(n-1)\beta(n-1) - f(n)A(n)\alpha(n), \qquad (1.14)$$

where $A(n)$ denotes the surface area of size-n nuclei, $f(n)$ the number density of size-n clusters, $\beta(n)$ and $\alpha(n)$ the fluxes per unit area per unit time of single molecule arriving at or leaving the size-n nuclei, respectively. The next assumption is that an equilibrium distribution of clusters $f_{eq}(n)$ can be es-

tablished in the bulk metastable phase. Because of microscopic reversibility, it can be written as

$$f_{eq}(n-1)A(n-1)\beta = f_{eq}(n)A(n)\alpha, \tag{1.15}$$

where α and β are assumed to be independent of n. Hence, $\alpha(n)$ can be eliminated from equation(1.14):

$$J(n) = \beta A(n-1) f_{eq}(n-1)\left[\frac{f(n-1)}{f_{eq}(n-1)} - \frac{f(n)}{f_{eq}(n)}\right]. \tag{1.16}$$

In the steady state, all fluxes are equal to a single constant flux J. By summing the following equations from $n = 2$ to $n = \Lambda$

$$\frac{J}{\beta A(n-1) f_{eq}(n-1)} = \frac{f(n-1)}{f_{eq}(n-1)} - \frac{f(n)}{f_{eq}(n)} \quad (n = 2, 3, \cdots, \Lambda), \tag{1.17}$$

we can obtain,

$$J = \frac{\dfrac{f(1)}{f_{eq}(1)} - \dfrac{f(\Lambda)}{f_{eq}(\Lambda)}}{\displaystyle\sum_{n=1}^{\Lambda} \frac{1}{\beta A(n) f_{eq}(n)}} = \frac{1}{\displaystyle\sum_{n=1}^{\Lambda} \frac{1}{\beta A(n) f_{eq}(n)}}. \tag{1.18}$$

Here Λ should be some large number so that we can assume $f(\Lambda) \ll f_{eq}(\Lambda)$ [8]. The hypothetical distribution function $f_{eq}(n)$ must have the form

$$f_{eq}(n) \propto \exp\left[-\frac{W_{\min}(n)}{k_B T}\right], \tag{1.19}$$

where $W_{\min}(n)$ is the minimum work needed to form a size-n cluster. $f_{eq}(1)$ is expected to be ρ_{tot}, the total number density of molecules. Therefore,

$$f_{eq}(n) = \rho_{\text{tot}} \exp\left[-\frac{W_{\min}(n)}{k_B T}\right] \tag{1.20}$$

The homogeneous nucleation rate is obtained by substituting (1.20) into (1.18):

$$J = \beta\rho_{\text{tot}} \left[\int_1^{\Lambda} \exp\left(\frac{W_{\text{min}}(n)}{k_B T} \right) \frac{1}{A(n)} dn \right]^{-1}, \tag{1.21}$$

where the summation is replaced by an integral.

To calculate the homogeneous nucleation rate, we should know the minimum work needed to form a nucleus. The minimum work can be written in general form,

$$W_{\text{min}} = \gamma A + (p - p')V' + n\left[\mu_{\text{liq}}(T, p') - \mu_{\text{vap}}(T, p)\right] \tag{1.22}$$

where γ is the surface tension or surface excess free energy. The symbols with a single prime denote quantities pertaining to the liquid phase, and the symbols without a prime denote the vapor phase. For incompressible embryos,

$$\mu_{\text{liq}}(T, p') - \mu_{\text{vap}}(T, p) = v'(p' - p). \tag{1.23}$$

Substitution of (1.23) into (1.22) yields

$$\begin{aligned} W_{\text{min}} &= \gamma A + n\left[\mu_{\text{liq}}(T, p) - \mu_{\text{vap}}(T, p)\right] \\ &= 4\pi r^2 \gamma - \frac{4\pi}{3} r^3 \rho' \Delta\mu \quad \text{(for a spherical droplet)}. \end{aligned} \tag{1.24}$$

A typical picture of the minimum work is shown in figure (1.1). The minimum work has a maximum as a function of r. Here and below, the values at the maximum is denoted by the asterisk. An embryo corresponding to

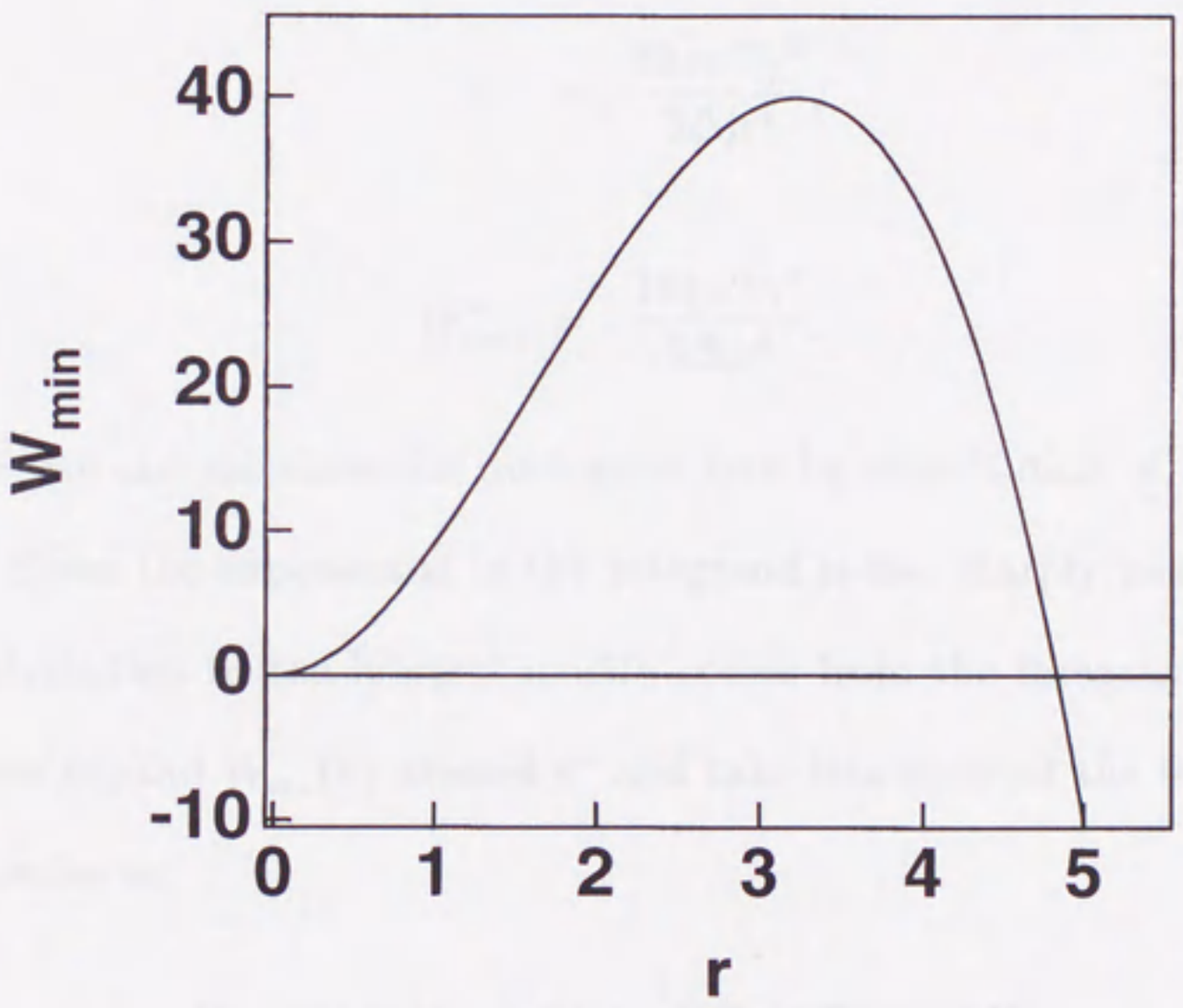

Figure 1.1: Minimum work to create a cluster of radius r from supersaturated vapor; schematic figure.

the maximum is called "critical embryo" or "critical nuclei", which is in unstable equilibrium. The size of the critical nucleus and minimum work are calculated from (1.24) as $(\partial W_{\min}/\partial r)_{r=r^*} = 0$:

$$r^* = \frac{2\gamma v'}{\Delta\mu}, \tag{1.25}$$

$$n^* = \frac{32\pi v'^2\gamma^3}{3\Delta\mu^3}, \tag{1.26}$$

$$W^*_{\min} = \frac{16\pi v'^2\gamma^3}{3\Delta\mu^2}, \tag{1.27}$$

Now, we can calculate the nucleation rate by substitution of (1.24) into (1.18). Since the exponential in the integrand is the sharply peaked at n^*, the contribution to the integral mostly comes from the integrand near n^*. Hence we expand $W_{\min}(n)$ around n^* and take into account the terms up to second order as,

$$W_{\min}(n) \approx W_{\min}(n^*) + \frac{1}{2}W''_{\min}(n^*)(n-n^*)^2. \tag{1.28}$$

Then we obtain the rate J as

$$J = \beta A(n^*)\sqrt{\frac{W''_{\min}(n^*)}{2\pi k_B T}}\rho_{\text{tot}} \exp\left(-\frac{W_{\min}(n^*)}{k_B T}\right). \tag{1.29}$$

Equations (1.24) and (1.27) lead to

$$J = 2\beta\rho_{\text{tot}}\sqrt{\frac{\gamma v'^2}{k_B T}} \exp\left[-\frac{16\pi v'^2\gamma^3}{3k_B T(\Delta\mu)^3}\right]. \tag{1.30}$$

If we assume the vapor phase to be ideal gas, we can use

$$\beta = \frac{p}{\sqrt{2\pi m k_B T}} \quad \text{for all} \quad n. \tag{1.31}$$

1.2.2 Nucleation in superheated liquids

The extension of the above formulation to the bubble nucleation is straightforward. The minimum work for bubble formation is generally written as,

$$W_{\min} = \gamma A + (p - p')V' + n' \left[\mu_{\text{vap}}(T, p') - \mu_{\text{liq}}(T, p)\right] \tag{1.32}$$

The symbols with a single prime denote quantities pertaining to the vapor phase, and the symbols without a prime denote the ambient liquid phase.

The last term on the righthand side of equation (1.32) corresponds to the chemical potential difference and has a complicated form. To evaluate this term, we assume that the vapor is an ideal gas. Thus we have

$$\mu_{\text{vap}}(T, p) = k_{\text{B}} T \ln \frac{p}{p_0} + \Psi(T) \tag{1.33}$$

$$n' k_{\text{B}} T = \frac{4\pi r^3}{3} p' \quad \text{for a spherical bubble,} \tag{1.34}$$

where $\Psi(T)$ is a function dependent only on temperature, and p_0 is a reference pressure.

For $\mu_{\text{liq}}(T, p)$, we estimate it using the chemical potential of corresponding vapor in equilibrium with the ambient liquid; the vapor pressure p^* is obtained by

$$\mu_{\text{vap}}(T, p^*) = \mu_{\text{liq}}(T, p) \tag{1.35}$$

Combining equations (1.35) and (1.33), we estimate $\mu_{\text{liq}}(T, p)$.

The minimum work for a spherical bubble is obtained by substituting equations (1.35), (1.33) and (1.34) into equation (1.32),

$$W_{\min}(r, p') = 4\pi r^2\gamma - \frac{4\pi r^3}{3}(p' - p) + \frac{4\pi r^3}{3}p' \ln\frac{p'}{p^*}. \tag{1.36}$$

Note that $W_{\min}$ for bubble formation is a function of two variables (T and p'). The bubble formation occurs beyond the saddle point of $W_{\min}$. The position of the saddle point is determined as

$$\begin{cases} \dfrac{\partial W_{\min}}{\partial p'} = 0 \\ \\ \dfrac{\partial W_{\min}}{\partial r} = 0 \end{cases} \Longrightarrow \begin{cases} p' = p^* \\ \\ p' - p = \dfrac{2\gamma}{r^*} \end{cases} \tag{1.37}$$

The height of free energy barrier to form a critical bubble is

$$W^*_{\min} = \frac{4\pi\gamma r^{*2}}{3}. \tag{1.38}$$

In a similar way to the previous section, we expand $W_{\min}(r, p')$ around the saddle point and take into account the terms up to second order as

$$\begin{aligned} W_{\min}(r, p') \approx\ & W^*_{\min} + \frac{1}{2}W_{rr}(r - r^*)^2 + \frac{1}{2}W_{pp}(p' - p^*)^2 \\ & + W_{rp}(r - r^*)(p' - p^*), \qquad (1.39) \\ =\ & \frac{4\pi\gamma r^{*2}}{3} - 4\pi\gamma(r - r^*)^2 + \frac{2\pi r^{*3}}{3p^*}(p' - p^*)^2, \qquad (1.40) \end{aligned}$$

where W_{rr}, W_{pp} and W_{rp} are second order derivatives at the saddle point. Since equation (eq:laplace) shows that the bubble is in mechanical equilibrium with its surroundings, $W_{\min}$ is written as [6, 9],

$$W_{\min} \approx \frac{4\pi\gamma r^{*2}}{3} - 4\pi\gamma(r - r^*)^2 B \tag{1.41}$$

where $B = 1 - (1 - p/p^*)/3$ is a numerical factor [9]. Substitution of equation (1.41) into (1.21) and replacement of the integration variable from n to r lead the expression of the rate J as

$$J = \rho_{tot}\sqrt{\frac{2\gamma}{\pi m B}}\exp\left[\frac{-16\pi\gamma^3}{3k_B T\,(p^* - p)^2}\right]. \tag{1.42}$$

Main assumptions we made in the derivation of equations (1.30) and (1.42) are

1. The surface free energy is estimated with surface tension of macroscopic surface. This assumption is usually called capillary approximation.

2. To eliminate the coefficient of backward process α, we use the hypothetical equilibrium nucleus density $f_{eq}(n)$, which obeys the Boltzmann distribution.

3. Nucleus distribution is independent of time, which is called steady state approximation.

1.3 Experiments

To evaluate the nucleation rate, it is necessary to count the number of generated nuclei. Contrary to the nucleation from vapor phase, in which light scattering technique is useful to detect the number and size of nuclei [10, 11, 12], it is still difficult to measure the rate of bubble formation in metastable liquid. Therefore, in most of bubble formation experiments, some superheat limit of liquids is measured.

There are two typical ways to realize a metastable state of liquid. One is to heat the liquid under constant pressure up to some temperature above the boiling point, and the other is to expand the liquid under constant temperature and make its pressure less than the saturated vapor pressure. The former is called superheat, and the latter overexpansion, but they correspond to the same metastable state from physical view point.

Let us explain the experiments by taking the superheating process for an example. The nucleation rate J strongly depends on the penetration depth into the metastabe state (temperature in the case of superheating); a schematic figure is shown in figure 1.2. The nucleation rate changes by many orders of magnitude across a very narrow temperature range. This steepness of J causes a sharp transition to explosive boiling. Thus we can define the kinetic limit of liquids, or superheat limit T_{sh}.

The nucleation rate J_{sh} corresponding to T_{sh} depends on various experi-

Table 1.1: Typical nucleation rates attainable with various experimental methods.

Method	$J(\text{cm}^{-3}\ \text{sec}^{-1})$
Bubble chember	$10^2 - 10^3$
Capillary tube	$10^5 - 10^6$
Droplet superheat	$10^{18} - 10^{23}$

mental methods. Typical values are shown in Table 1.1.

Now, let us briefly describe several experimental methods. Details are reviewed in [13] and [14]; data are also compiled there.

1.3.1 Superheating measurements

In the pulse heating method, a short pulse of electric current is imposed on a wire of small diameter immersed in a test liquid. Bubble formation in the test liquid is detected by the rising rate of temperature due to the change of heat transfer rate. Since the electric resistance of the wire depends on its temperature, the resistance measurement gives $T_s h$. There are several error sources; spatial nonuniformities in the wire temperature, poor reproducibility of the calibration of temperature dependence of the wire resistance, and the temperature fluctuations caused by bubble formation.

The capillary tube method uses a capillary tube filled with a test liquid. It is heated under constant pressure, and bubble formation is detected by audible sound. Three major sources of error associated with the method are nucleation on capillary walls, thermal lag between the test liquid and the

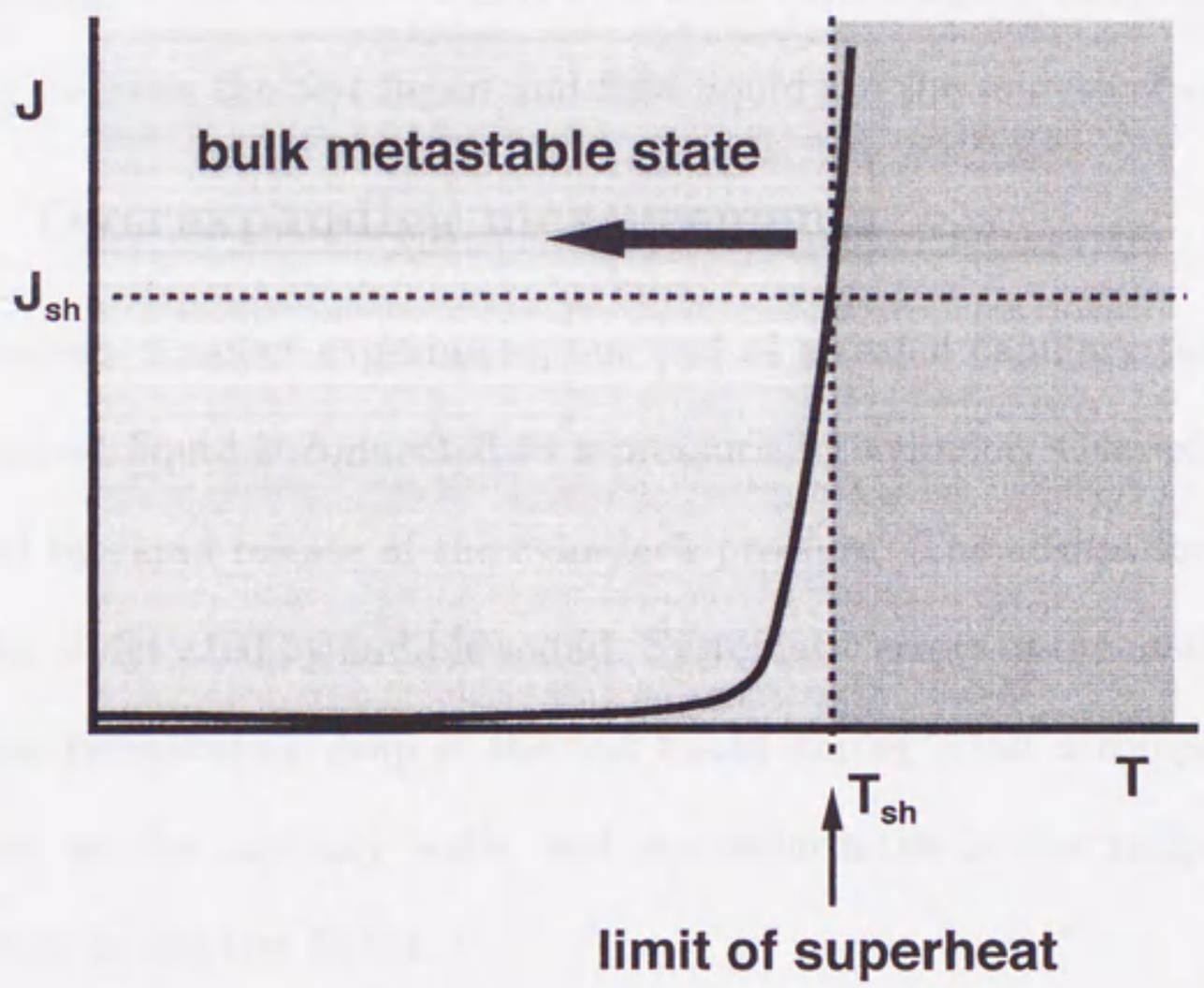

Figure 1.2: Schematic variation of nucleation rate as a function of temperature. T_{sh} is the limit of super heat which corresponds to the nucleation rate J_{sh}.

environment, and nonuniformities in the test liquid.

The droplet superheating technique consists of a suspended droplet of a test liquid(volatile) in a immiscible field liquid (nonvolatile). A vertical temperature gradient is imposed on the field liquid. When the field liquid is denser than the test liquid, the droplet rises vertically, and bubble formation occurs at some height. The bubbles are detected by audible sound. Underheating of the droplet caused by a finite heat transfer rate, and finite solubility between the test liquid and field liquid are the sources of error.

1.3.2 Overexpanding measurements

In the bubble chamber experiment, one end of a sealed capillary tube containing a test liquid is connected to a pressurizing cylinder. Overexpansion is created by rapid release of the cylinder's pressure. The abrupt formation of bubbles is detected by audible sound. Systematic errors of the method are due to the temperature drop of the test liquid during rapid decompression, nucleation on the capillary walls, and nonuniformities in the temperature distribution in the test liquid.

Recently, Ohde et al. adopt a Berthelot tube method to maintain a test liquid under a large negative pressure [15]. By repeating the expansion and compression, one can remove existing heterogeneous nuclei.

1.3.3 Measurements of nucleation rate

Although nucleation rate estimation is difficult, two different approaches have been tried.

One is to measure the "life-time" of the matastable state, and a couple of works were reported [14, 16, 17]. Recently, a more direct method is used in a pulse heating apparatus [18], in which the number of generated bubbles is counted by an optical microscope. To improve the temperature uniformity, they adopt a a small film heater is used in stead of a wire.

1.4 The Aim of This Work

While nucleation processes in vapor phase have been studied from various viewpoints (from microscopic to macroscopic) and comparisons of experimental results with theoretical predictions are well advanced, less attention has been paid to bubble formation in spite of its scientific and practical importance. There are a number of reasons for this situation. In experiments, to remove the effects of impurities and to prevent heterogeneous nucleation at the boundaries are difficult. Also in a theoretical aspect, rigorous treatment of a microscopic bubble is difficult because the classical theory contains several assumptions described in section 1.2. Evaluation of hydrodynamic effects of ambient liquids and interactions among generated bubbles are also complicated.

Molecular simulation approach provides another method to explore microscopic mechanisms of such phase transition processes. In particular, by using molecular dynamics (MD) technique, one can pursue the motion of each molecule directly; analyzing molecular trajectories and other time-dependent system properties, it is expected that we can understand the mechanism of these fluid phase transitions on molecular level.

Thus I adopt the MD method to investigate the bubble formation phenomena. I focus on two different systems. One is a pure liquid in an overexpanded state, where a spontaneous bubble formation (cavitation) is expected.

The other is a binary liquid mixture, where I use a liquid with dissolved gas. In the latter case, a degassing process like bubbles of carbonated water is expected, the mechanism of which may be different from the cavitation process.

The aims of this work are:

1. To examine the applicability of a MD method to determine the stability limit of liquids.

2. To estimate the nucleation rate and compare it with theoretical prediction.

3. To examine whether "critical nucleus" exists or not, and if it exists, to develop a method to estimate its size.

4. To investigate the molecular mechanism of bubble formation, and make comparison of the two processes, cavitation and degassing.

Chapter 2

UNARY LIQUIDS –CAVITATION–

2.1 Introduction

In this chapter, I investigate bubble formation in unary liquids. In many practical situations, bubble formation is often initiated at impurities or on solid boundaries(i.e., heterogeneous nucleation). Understanding of homogeneous bubble nucleation is important as fundamentals of heterogeneous and homogeneous nucleations.

Far below the critical temperature, liquids can withstand negative pressure (tensile force). In this case, the bubble formation in metastable liquids is often called cavitation which is relevant to designing a high-performance ship propeller [1, 19]; since bubbles reduce the driving force, it is required to design a propeller not to generate large negative pressure. For that purpose, evaluation of metastablity limits is important.

Let us consider the equation of state for Lennard-Jones fluid [20], the

isotherm of which is shown in figure 2.1. In this figure, A and D respectively corresponds to the coexisting liquid and vapor which are determined by Maxwell's equal area rule. The states B and D are the liquid spinodal and the vapor spinodal, respectively. The metastable states of liquid the states exists between A and B along the isotherm. The liquid at a stable point can be expanded beyond the state A which corresponds to the boiling point, but can never go over the state B without phase transition. In a state between B and C, the isothermal compressibility is negative ($\kappa_T \equiv v^{-1}(\partial v/\partial P)_T < 0$), and thus the system in the region is inherently unstable as shown in (1.13). Figure 2.2 shows isotherms and the spinodal curve. The spinodal curve is projected to the ρ-T and the T-P plane. (figures 2.3,2.4)

In principle, liquid quenched to a metastable state undergoes a phase transition. However, shallow quenching is not sufficient to cause phase transition, because the work required for the creation of surface is larger than the reduction of the free energy of the phase change. For example, it is well known that liquids can withstand modest tensile force, or negative pressure. In the case of liquid-to-vapor phase transition, if the quenching is sufficiently deep, the liquid undergoes explosive phase transition to vapor, which is called vapor explosion for the case of positive pressure, or cavitation for the case of negative pressure [1, 4, 13, 21].

The purpose of this chapter is to investigate the dynamics of bubble formation in unary liquids. With this objective, I have carried out molecular

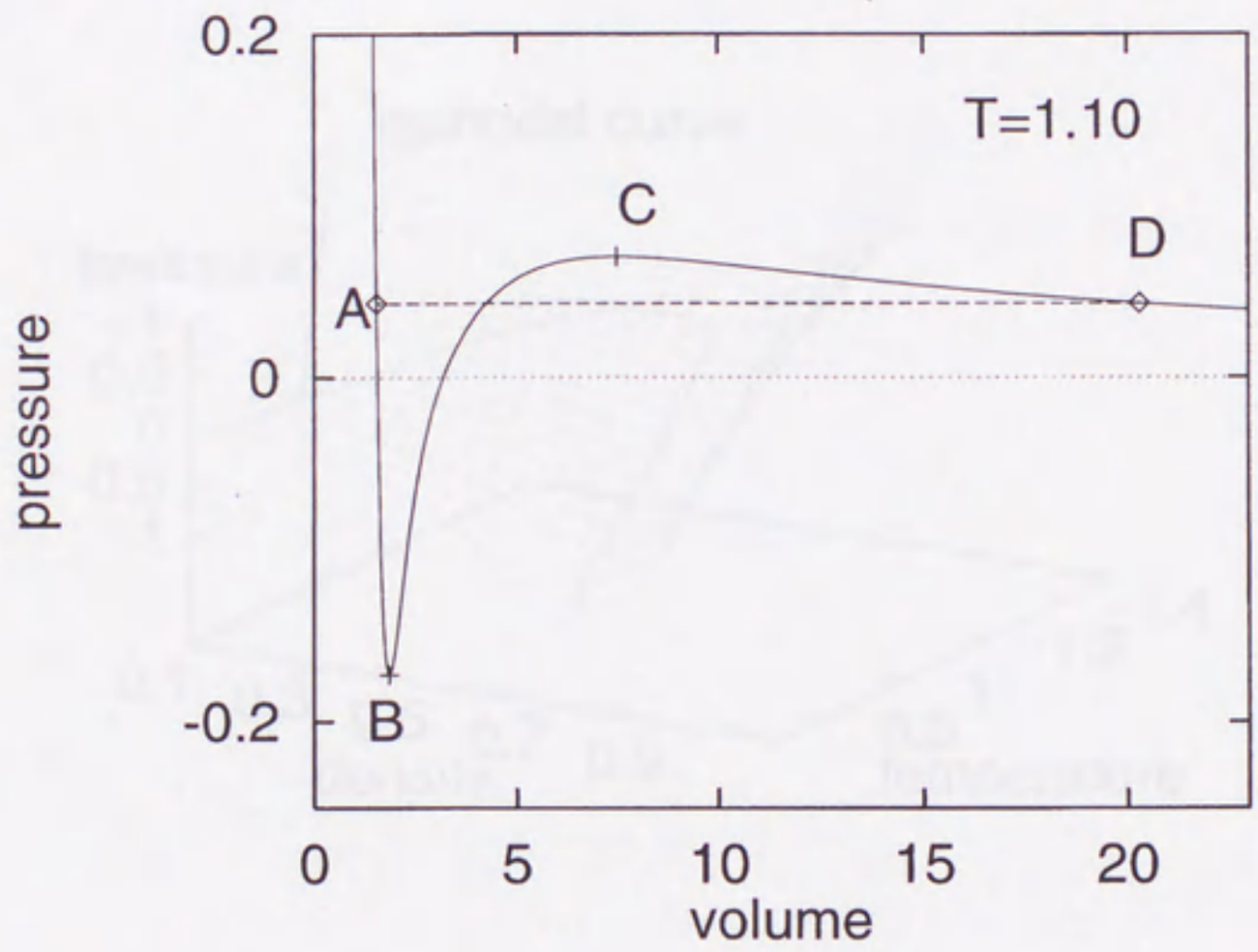

Figure 2.1: The isotherm of the Lennard-Jones fluid [20] at $T = 1.1$

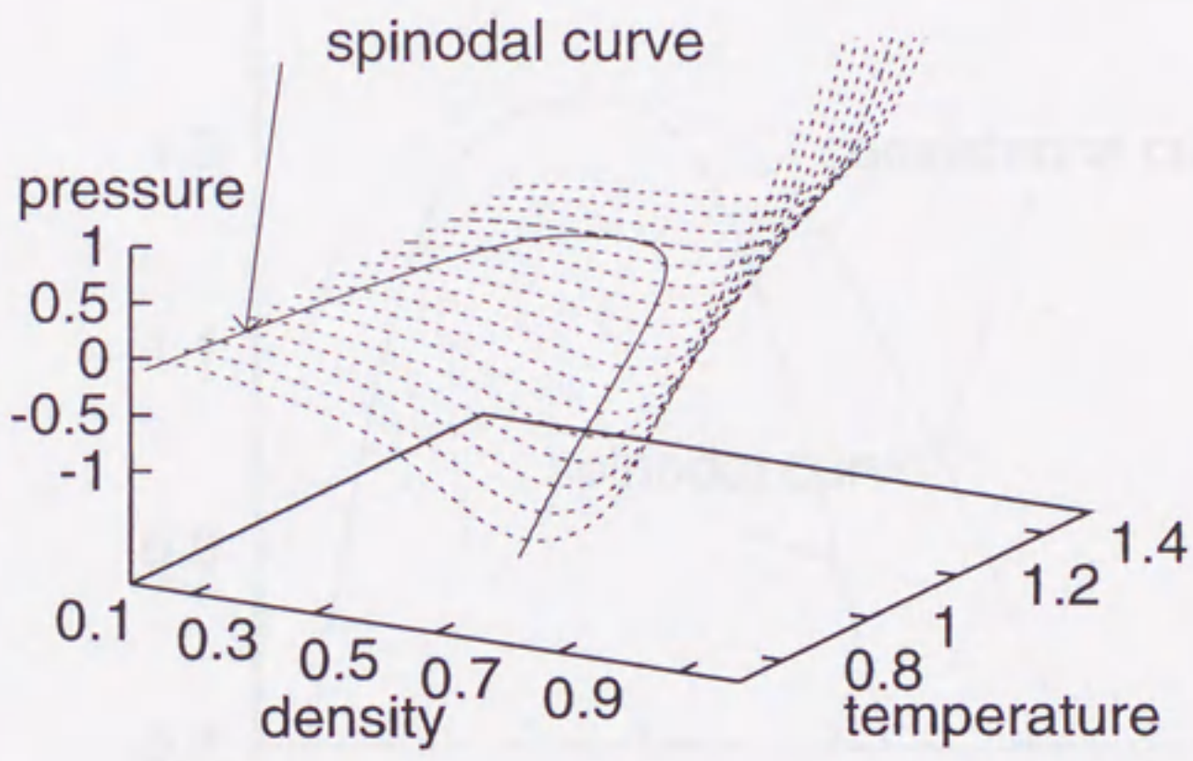

Figure 2.2: The equation of state and the spinodal curve of the Lennard-Jones fluid [20]

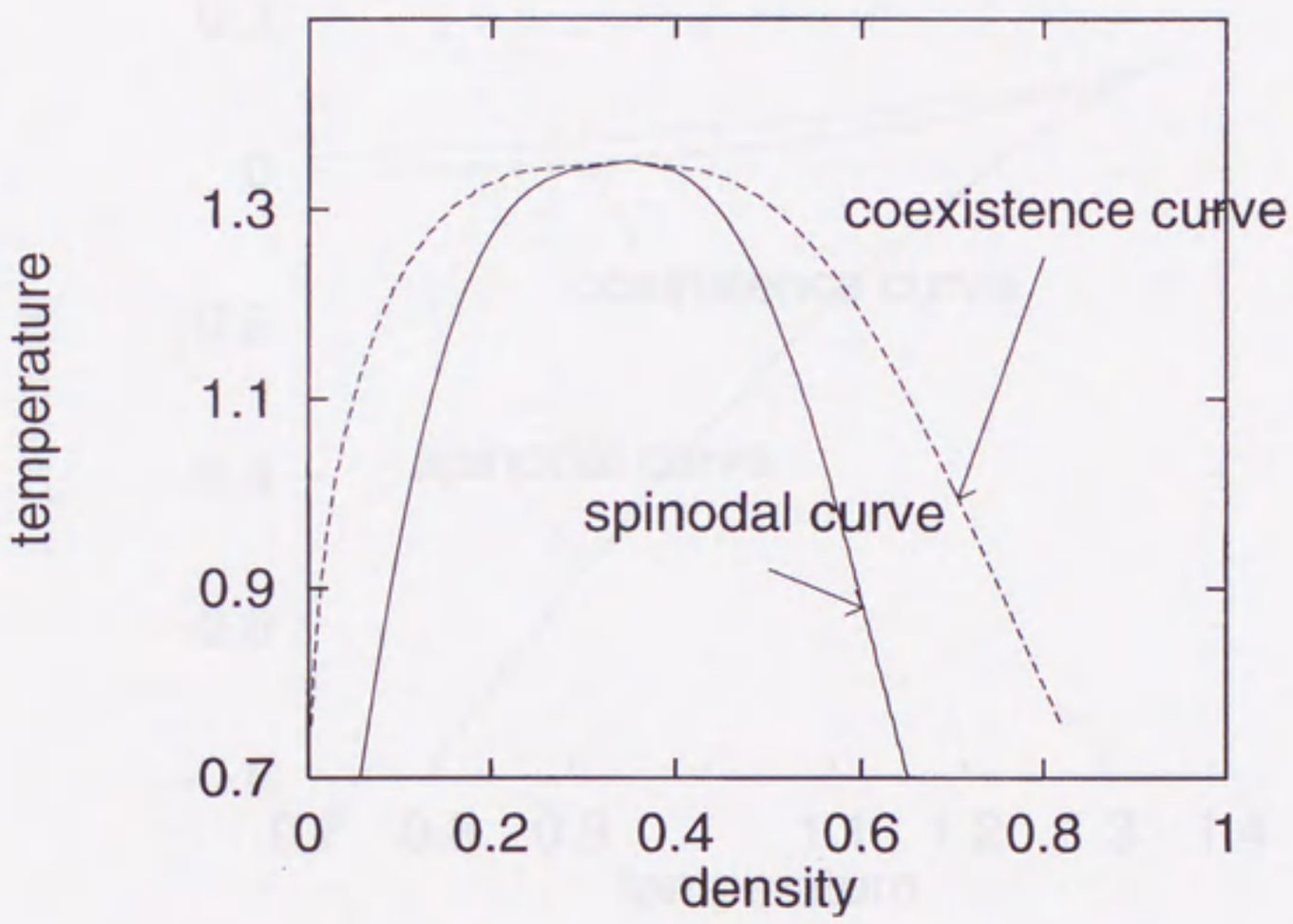

Figure 2.3: The spinodal line of Lennard-Jones fluid [20] ; ρ-T projection

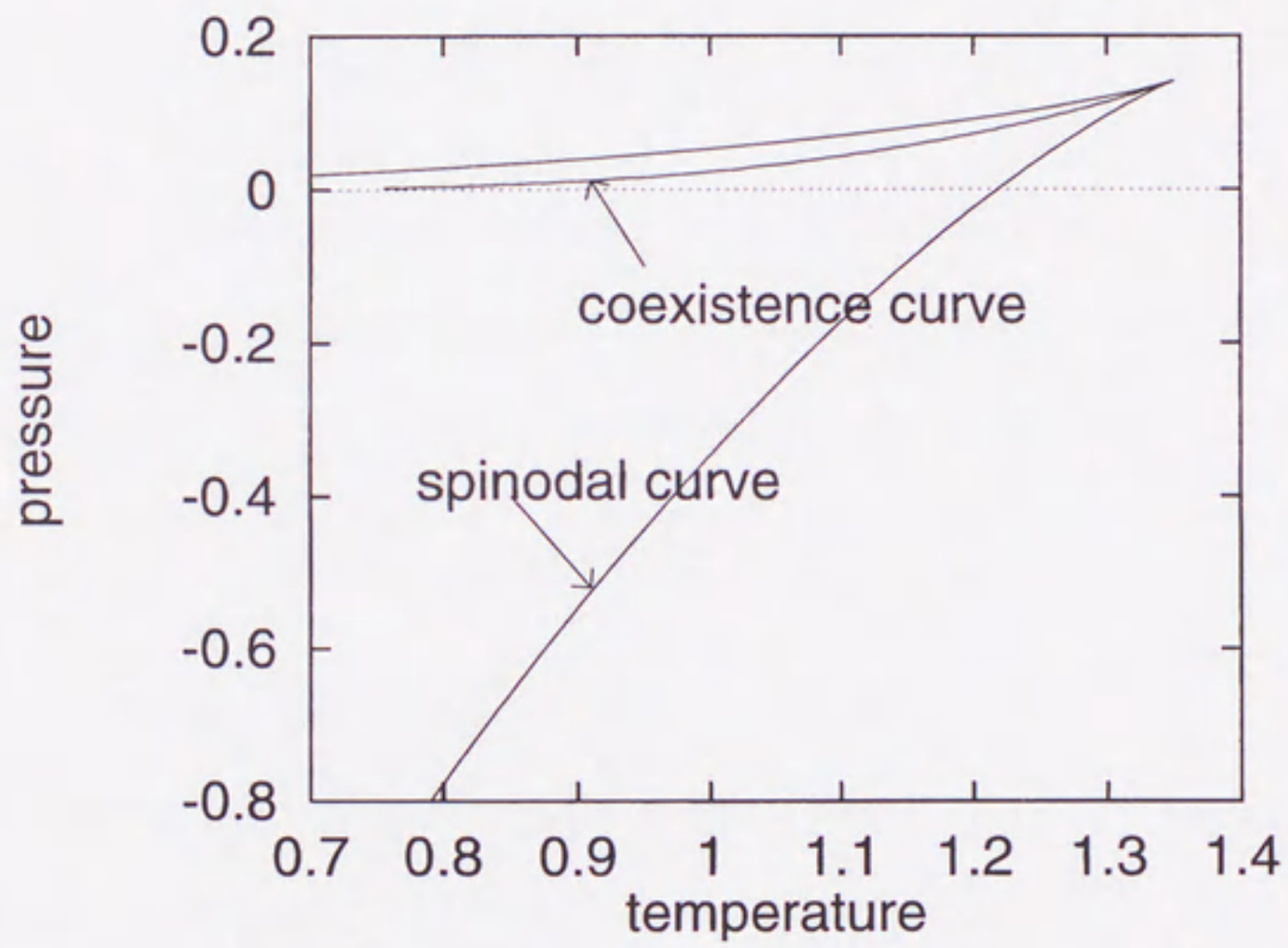

Figure 2.4: The spinodal line of L-J fluid [20] ; T-P projection

dynamics(MD) simulation of a Lennard-Jones fluid for fairly large systems, and have observed the inception of vapor phase (or nuclei of bubbles) in the bulk liquid phase.

Table 2.1: The table of units(for argon)

values	units	for argon
length	σ	3.4×10^{-10} m
mass	m	6.63×10^{-23} kg
time	$\tau = \sqrt{m\sigma^2/\epsilon}$	2.14 ps
temperature	ϵ/k_B	120 K
pressure	ϵ/σ^3	42.2 MPa (416 atm)

2.2 Simulation Method

To investigate the bubble formation processes, I carried out microcanonical MD simulations. The system treated here consists of 10,976 particles. These particles interact each other via the Lennard-Jones potential:

$$\phi_{\rm LJ}(r) = 4\epsilon\left[\left(\frac{\sigma}{r}\right)^{12} - \left(\frac{\sigma}{r}\right)^{6}\right], \tag{2.1}$$

where r is the distance between interacting molecules.

I performed our calculation with reduced units, i.e., length in σ, energy ϵ, and mass m (mass of a particle). Thus, the time unit is $\tau = \sqrt{m\sigma^2/\epsilon}$, and the pressure unit is $\epsilon\sigma^{-3}$. For reference, the unit values for fluid argon are $\sigma = 3.4 \times 10^{-10}\,\mathrm{m}$, $\epsilon/k_B = 120\,\mathrm{K}$, and $\tau = 2.14\,\mathrm{ps}$. The value of the pressure unit is 42.2 MPa.

The time step of the simulation is $\Delta t = 0.0025$, and the cutoff length is 4.0 in these units. Long range corrections were made for potential energy and pressure assuming that the liquid structure is uniform beyond the cutoff radius.

The initial temperature of the system is 0.8. The critical temperature is 1.35 and the triple point temperature is 0.67. The equilibrated initial configurations were expanded uniformly and instantaneously with various expansion ratios. After this adiabatic expansion, I continued microcanonical MD simulation.

I did not control the system temperature, because the heat capacity of the surrounding liquid is sufficiently large. In the case of vapor phase nucleation (cluster formation), the temperature of the generated clusters is higher than the surrounding vapor due to the latent heat release[22]. In the bubble formation case, however, the temperature of generated bubbles (or vapor inside) is not important. The temperature of surrounding liquid is slightly raised (typically 0.2) because the liquid is contracted during the bubble growth, but this small temperature increase affects little the dynamics of bubble formation.

2.3 Results

2.3.1 Limit of metastability

If bubbles are formed, the system pressure is expected to increase. I first monitored the time development of the system pressure, and found three types of behavior for fairly small change of the density($\sim$ 1 %). Figure 2.5 shows the three types of pressure change corresponding to metastable state($\rho = 0.708$), limit of metastability($\rho = 0.694$), and unstable state($\rho = 0.690$). In the case of $\rho = 0.690$, pressure immediately increases toward positive value. This increase implies that bubbles appear in the liquid. The case of $\rho = 0.694$ is more interesting, in which pressure was maintained in the first stage, and then increased in the second stage. After such waiting time, one bubble (in this case) appeared. The corresponding snapshot is shown in figure(2.6). In a system having higher density than these, I did not observe bubble formation at least in our simulation time (200τ). Such distinction of conditions between metastable liquid and bubble formation is sufficiently clear to show the kinetic limit points on the phase diagram.

I used various initial configurations, and obtain several points of kinetic limit of metastability as shown in figure(2.7) and figure(2.8). Several empirical equations of state (EOS) are reported about the Lennard-Jones fluid system, with which we can calculate the spinodal line. In figure(2.7) and figure(2.8), the line based on EOS of Nicolas *et al.*[20] is shown; our MD

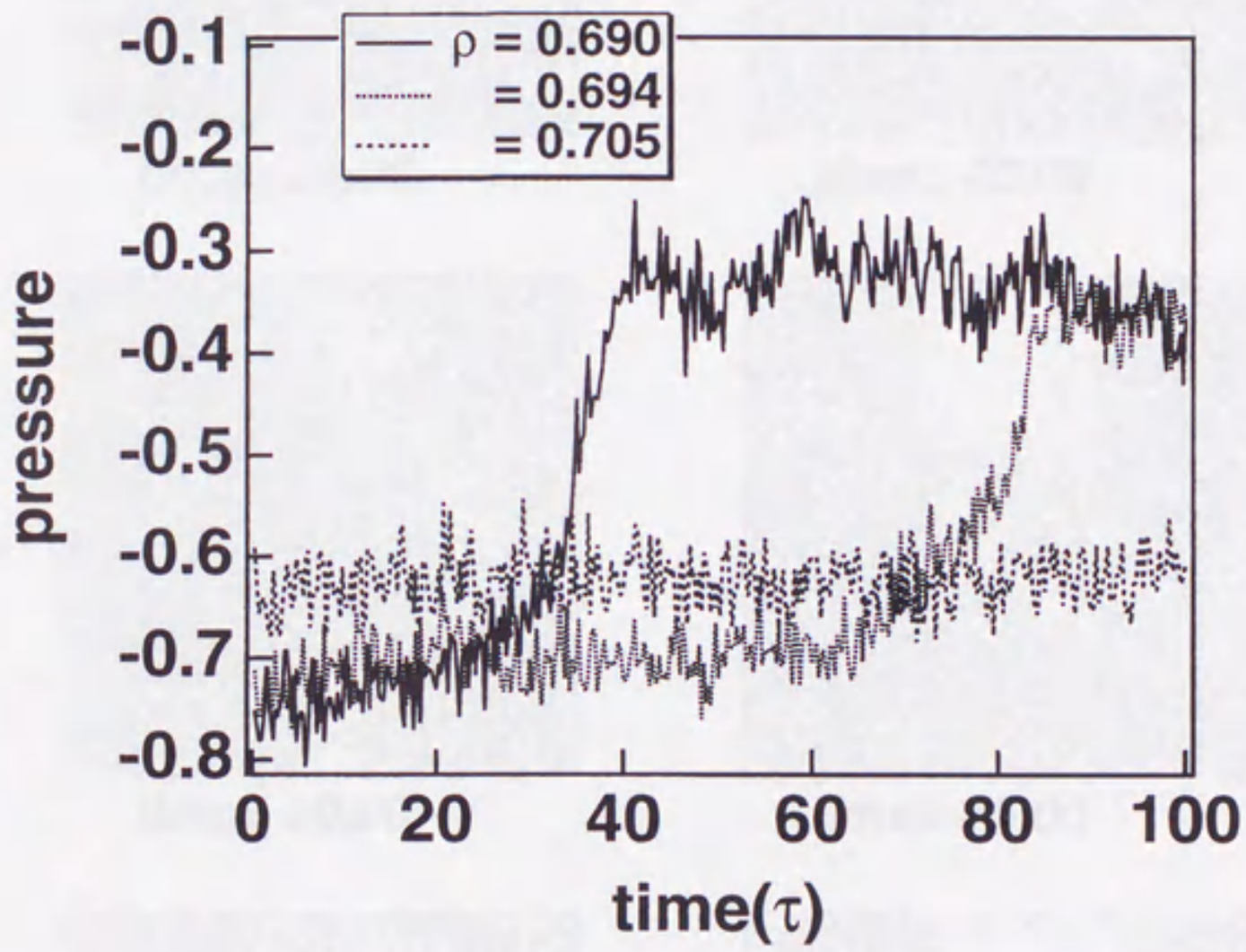

Figure 2.5: The time developments of the system pressures. $\rho = 0.694$ is a limit of stability of the liquid.

Figure 2.6: Snapshots of the unary liquid. The 3-dimensional system is divided into 12 slices and one of them is shown sequentially.

points are near but above the line. More recently obtained EOS (for example, [23]) gives a similar result at low temperature region. The difference between EOS and our MD simulation may be important, but considering the accuracy of EOS near the spinodal region, I do not discuss it here.

2.3.2 Nucleation Rate

Near this kinetic limit, a rapid growth of a bubble after the waiting time was observed, which meant the size of the bubble becomes larger than critical one. Hence one can obtain nucleation rate $J_{\rm sim}$ from the waiting time $\tau_{\rm w}$ as follows:

$$J_{\rm sim} = \frac{1}{\tau_{\rm w} V}, \tag{2.2}$$

where V is the system volume. The obtained value is $J_{\rm sim} \simeq 1.53 \times 10^{29} {\rm cm}^{-3} {\rm s}^{-1}$.

On the other hand, a classical nucleation theory [9] predicts

$$J_{\rm class} = \rho_l \sqrt{\frac{2\gamma}{\pi m}} \exp\left[\frac{-16\pi\gamma^3}{3k_{\rm B}T\left(P_l - P_v\right)^2}\right], \tag{2.3}$$

With parameters of argon fluid at corresponding temperature, the calculated value is $J_{\rm class} \simeq 1.17 \times 10^{12} {\rm cm}^{-3} {\rm s}^{-1}$. Thus, $J_{\rm sim}$ is 17 orders of magnitude lager than $J_{\rm class}$. Such underestimation of the rate of the classical nucleation theory has been previously pointed out by Zeng and Oxtoby [24, 25, 26], who state that the free energy barrier of bubble formation remains finite near the spinodal region in the approximations of the classical theory [27, 28, 29].

Quantitatively speaking, the difference (17 orders of magnitude) between the simulational system and the theoretical prediction may be overestimated.

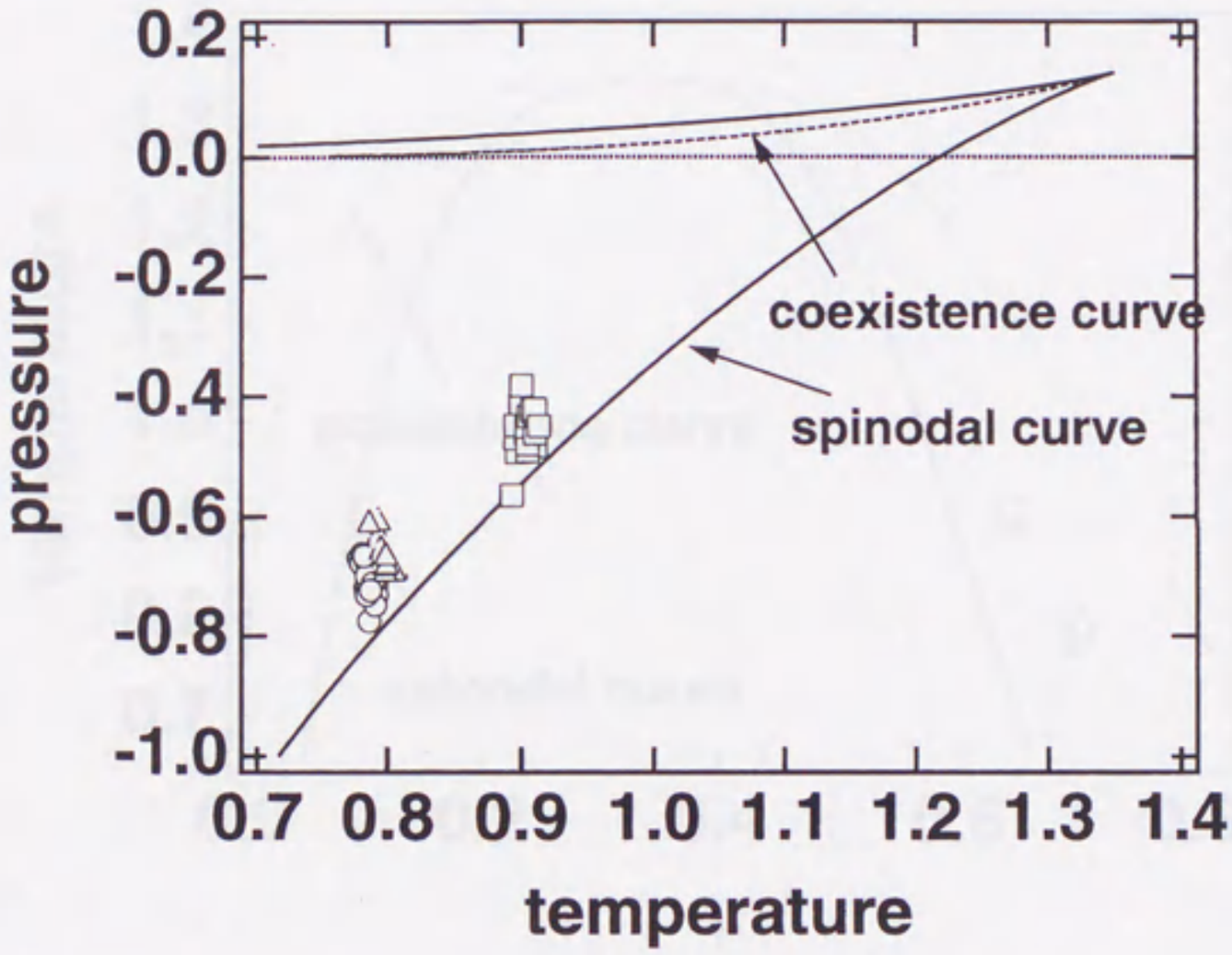

Figure 2.7: The stability limits shown on the T-P phase diagram for the Lennard-Jones fluid.

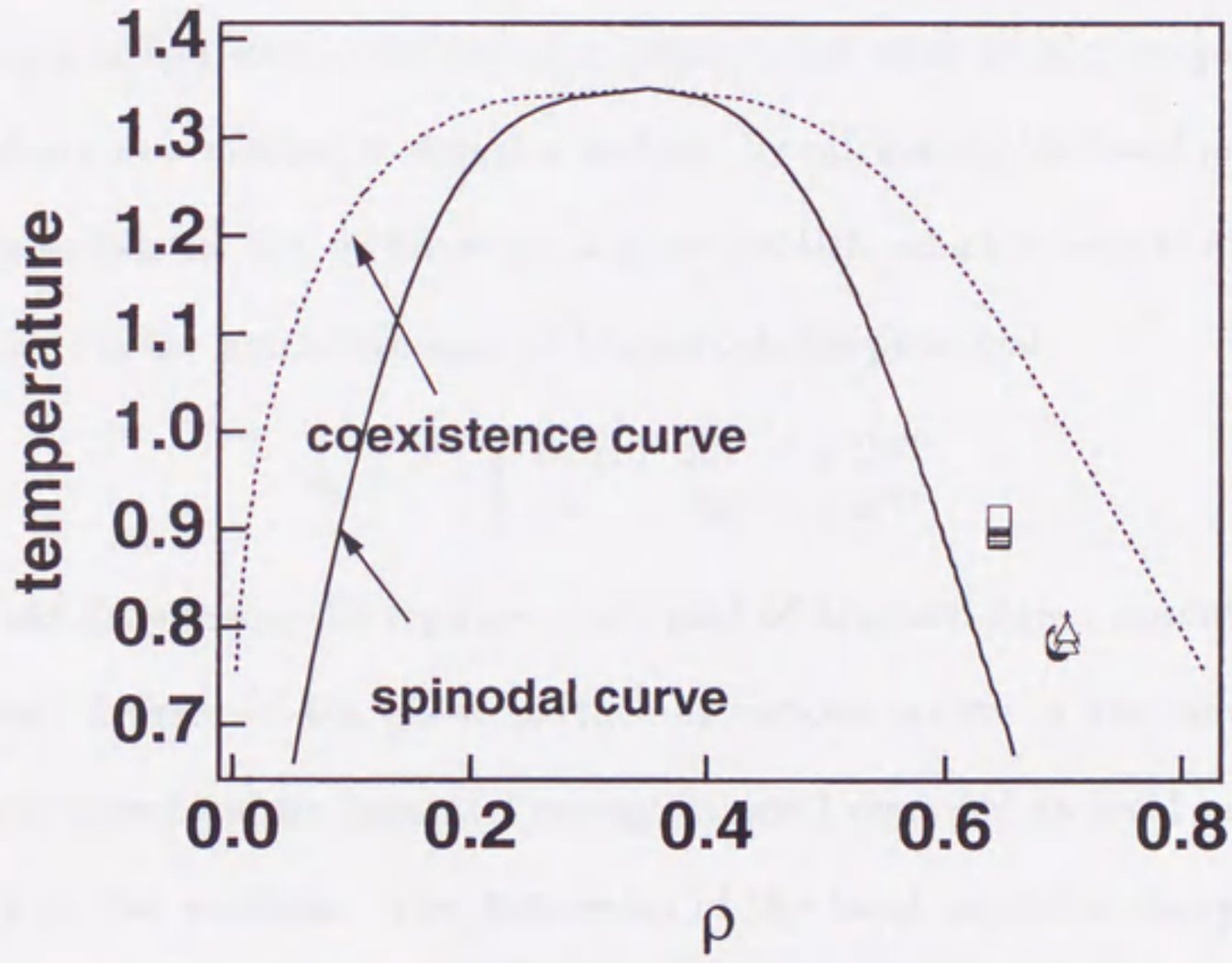

Figure 2.8: The stability limits shown on the ρ-T phase diagram for the Lennard-Jones fluid.

There are strong hydrodynamic effects in the system; once density fluctuations form a bubble, it generates shock waves, and the propagated waves may suppress further fluctuations. In other words, the system size I use here may not be large enough to realize the extensively of the phenomena.

2.3.3 Growth of Bubble

As shown in figure2.6, definition of a bubble is not clear at microscopic scale. I develop a new method to detect a 'bubble' by calculating the local potential energy as follows. Let us introduce a ghost particle which interacts with real particles via the attractive part of Lennard-Jones potential:

$$\phi_{\rm att}(r) = \begin{cases} \phi_{\rm LJ}(r) & \text{for} \quad r > 2^{1/6} \\ -\epsilon & \text{for} \quad r < 2^{1/6} \end{cases} \tag{2.4}$$

To avoid divergence, the repulsive core part of Lennard-Jones potential was omitted. I inserted the ghost particle at various points in the simulation cell and calculated its potential energy, which I regarded as local potential energy at the position. The histogram of the local potential energy after bubble formation is shown in figure(2.9), from which a threshold of -2.5 seems appropriate to define the bubble region. An equi-potential surface is shown in figure2.10, which captures well the shape of the bubble. The volume of a bubble is plotted against time in figure(2.11), which shows the growth of the bubble. I clearly distinguish two stages, i.e., growth–shrinkage period and explosive growth period. In the classical picture, the bubble in former period seems to be sub-critical and undergoes fluctuations. At this

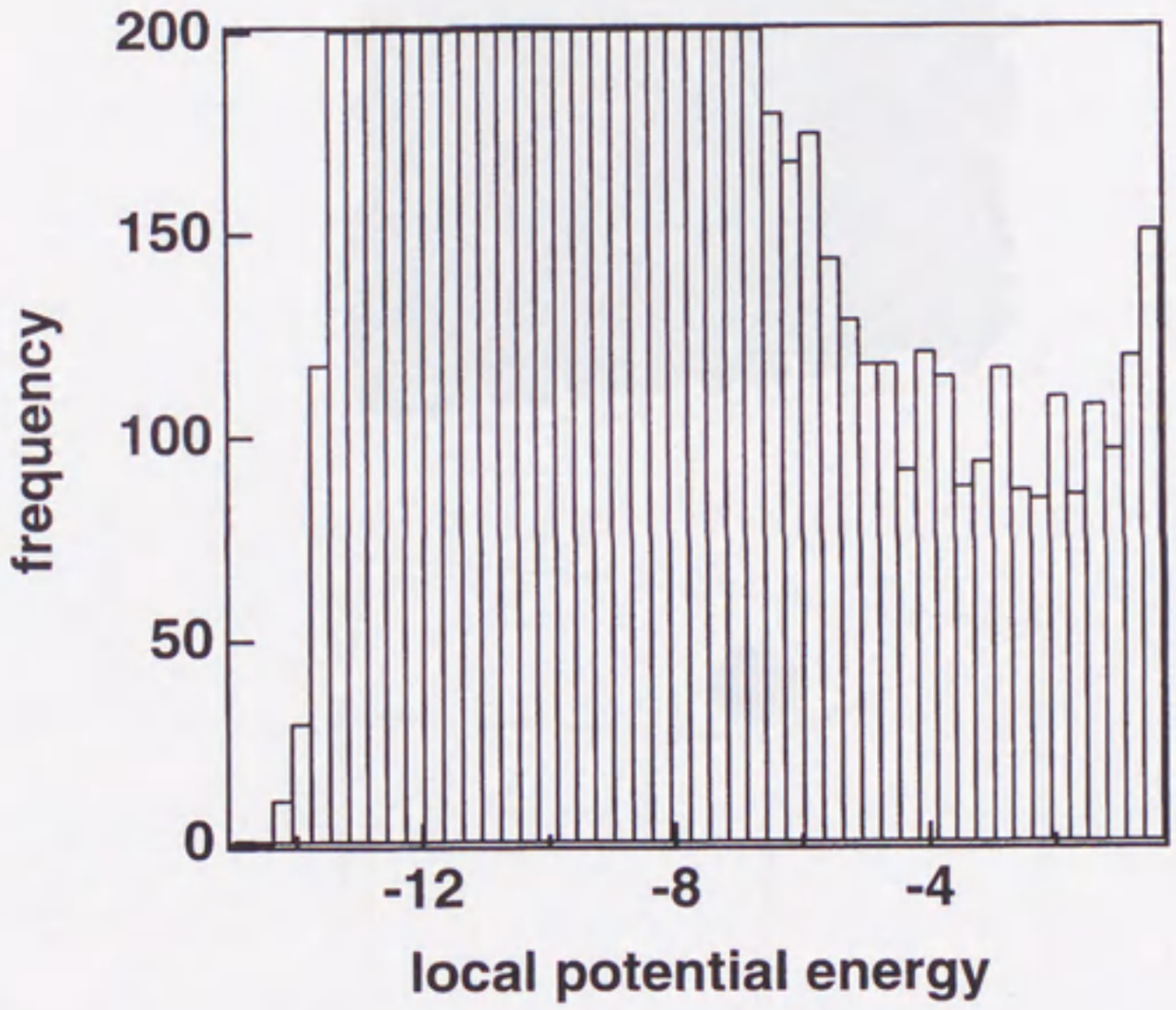

Figure 2.9: The histogram of the local potential energy.

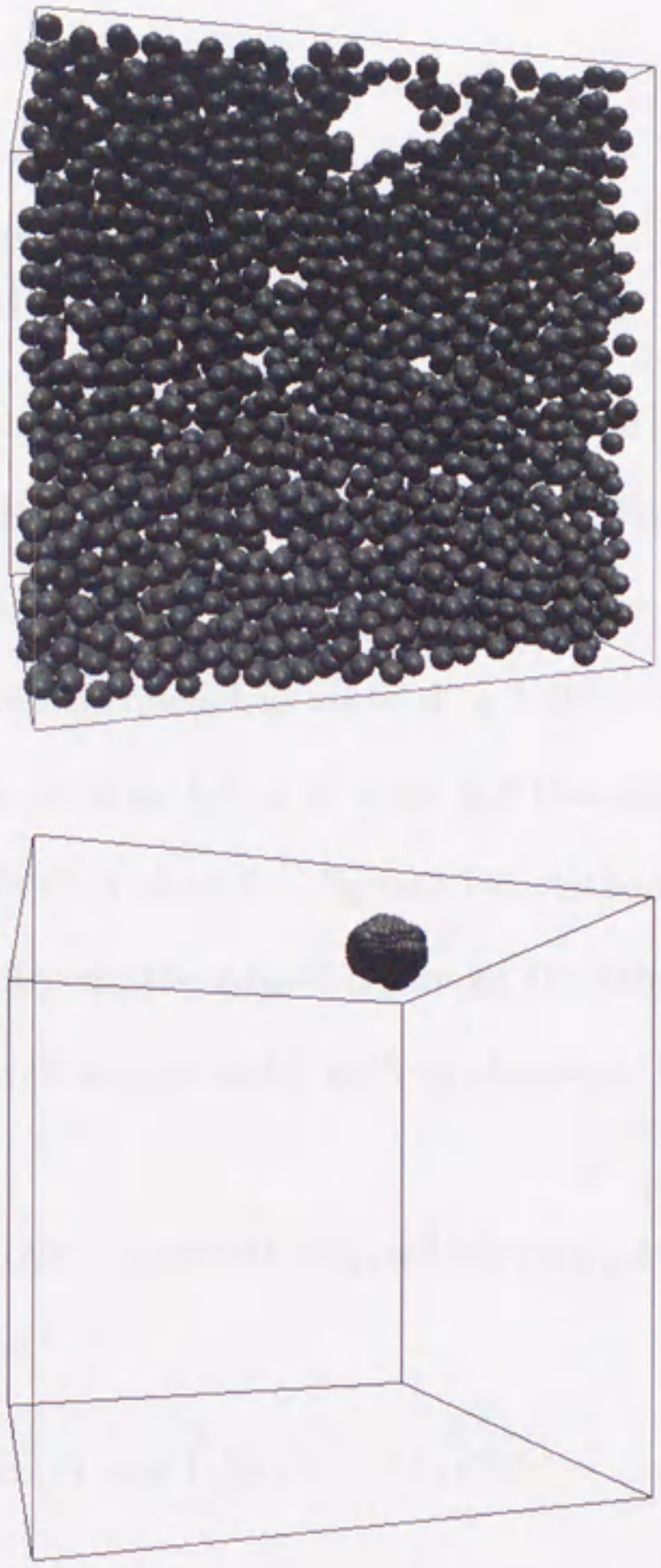

Figure 2.10: Snapshot of bubble(top) and the corresponding equi-potential surface(bottom).

stage the radius of bubble oscillated around 1, which corresponds to the critical size of the bubble. Once the bubble grows beyond the critical size, it grow up explosively.

/clearpage

2.3.4 Radial distribution function and isothermal compressibility

To investigate the structural difference between matastable liquid and normal one, I calculated the radial distribution function (RDF). Four liquid samples (three in metastable state and one in normal state) are used, which are shown in figure2.13. In the deepest quenched state **d**, a bubble is formed after a finite waiting time; the analysis below is done for the uniform metastable liquid samples (**a**–**c**). RDF is shown in figure2.14. Although the degree of metastability is quite different, their RDF is almost the same, including that of normal liquid. However, a systematic shift is observed; the overall shape moves to larger r.

To evaluate the difference quantitatively, we introduce a residual function $\Delta n(r)$ defined as follows:

$$\Delta n(r) = \rho \int_0^r [g(r') - 1] 4\pi r'^2 dr'. \tag{2.5}$$

If we use grand canonical ensemble, $\Delta n(r)$ is related to the isothermal compressibility κ_T as

$$\rho k_{\mathrm{B}} T \kappa_T = 1 + \rho \int_0^\infty [g(r') - 1]\, 4\pi r'^2 dr' = 1 + \Delta n(+\infty). \tag{2.6}$$

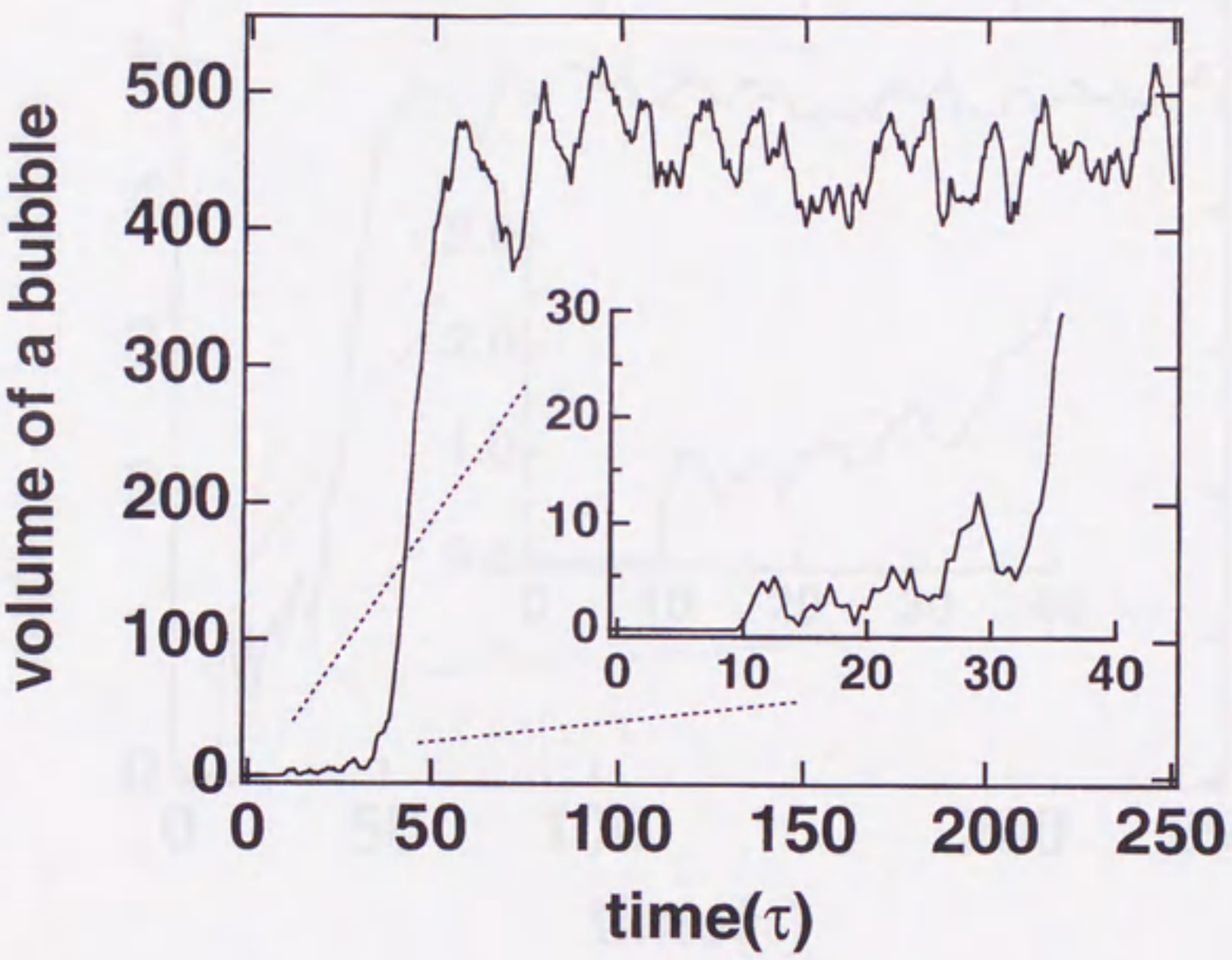

Figure 2.11: The time development of volume of a bubble

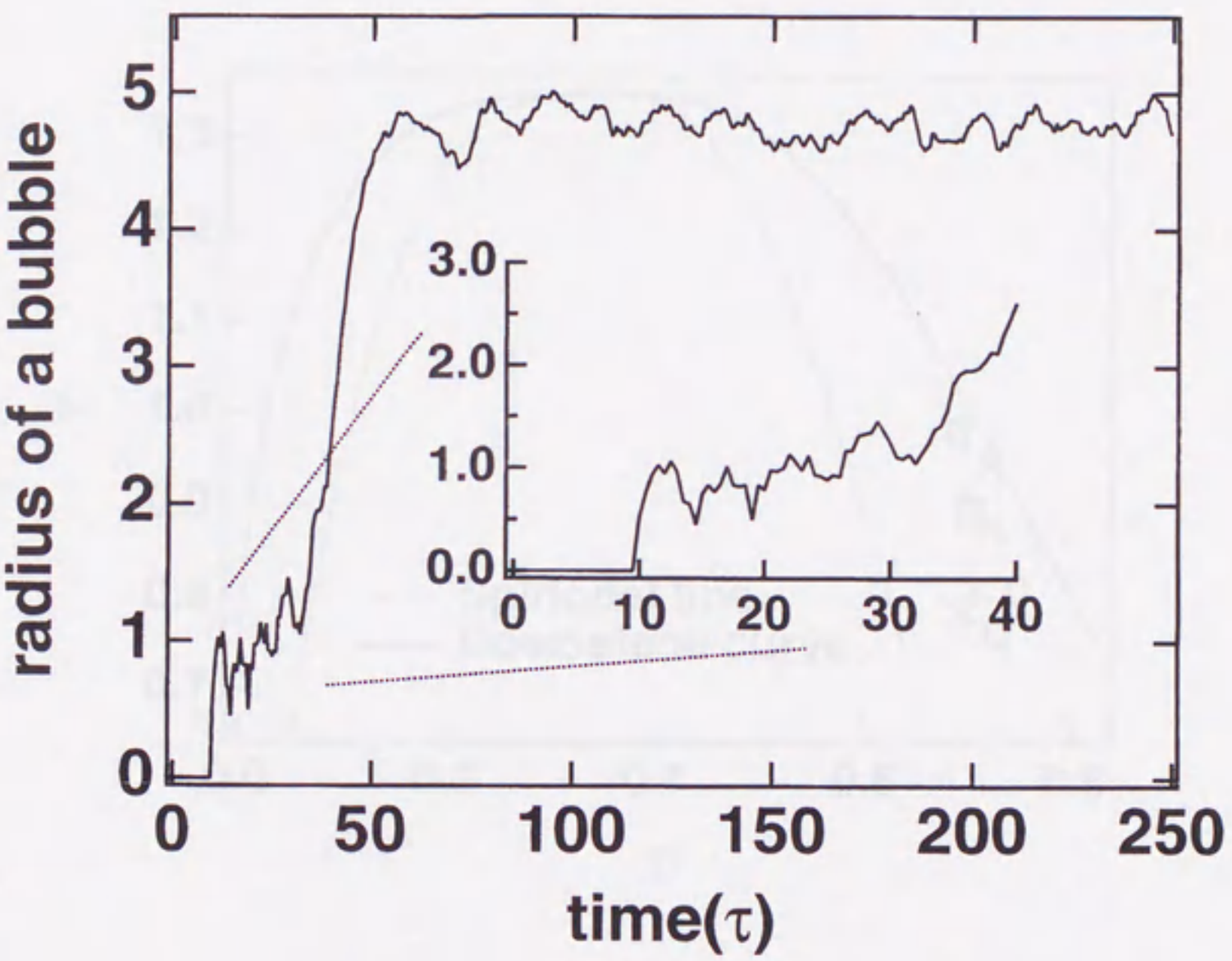

Figure 2.12: The time development of radius of a bubble

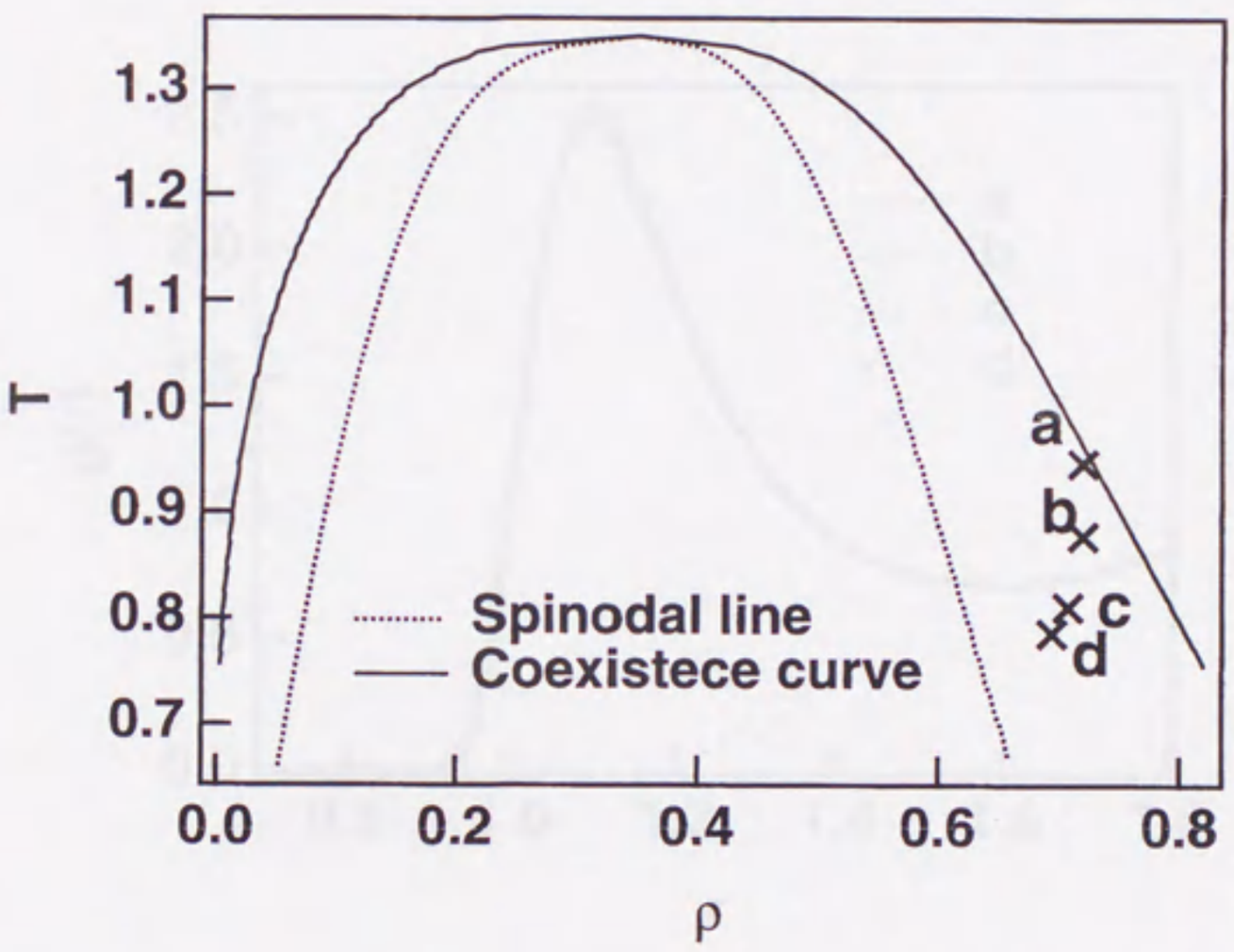

Figure 2.13: Simulated states in metastable region

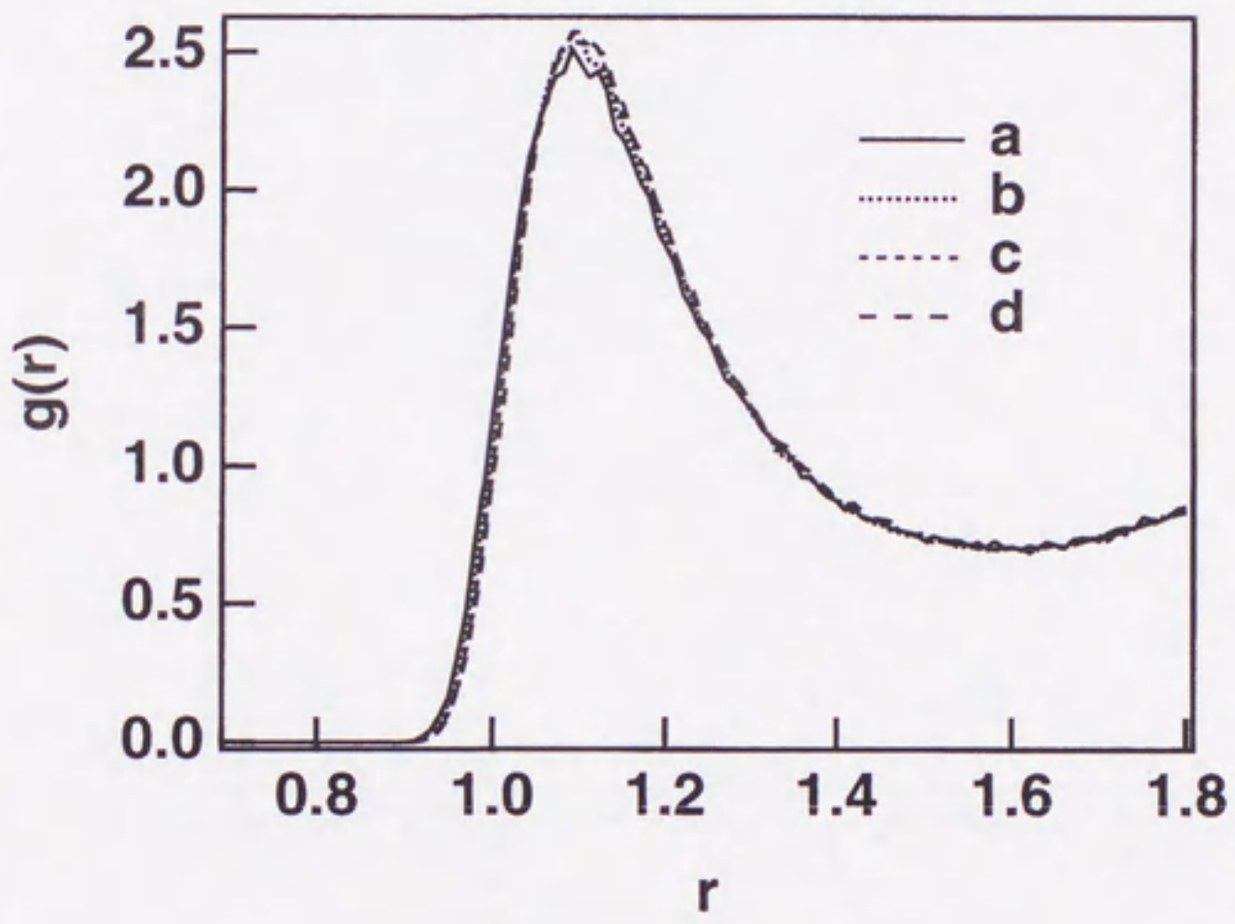

Figure 2.14: The radial distribution function

Since this simulation is done in microcanonical ensemble and the system is finite, it is difficult to take the limit of calculated $\Delta n(r)$ to evaluate κ_T. However, $\Delta n(r)$ converges at large $r \simeq 8$, I estimate κ_T with this plateau value. Figure)2.15 shows the density dependence of κ_T. It can be seen that the isothermal compressibility increases with approaching to kinetic limit of metastability; note that the temperature of each state is slightly different.

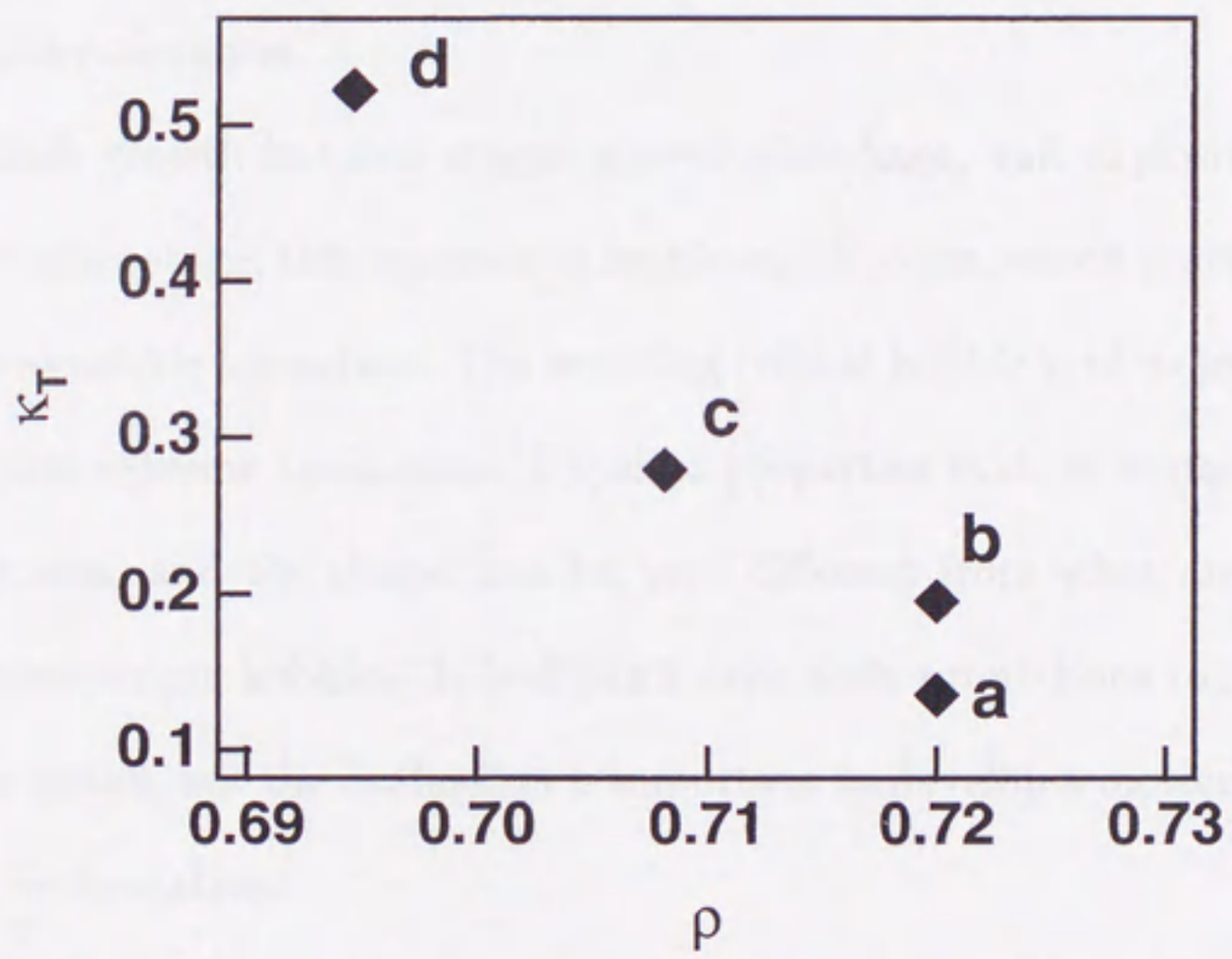

Figure 2.15: The isothermal compressibility

2.4 Discussion

In this chapter, I found using MD simulation the kinetic stability limit of liquid and observed bubble formation at this limit. From the waiting time for a single bubble to form, nucleation rate is calculated, which is much larger than the rate of classical nucleation theory. One of the theoretical defects, i.e., remaining free energy barrier near spinodal region, seems the cause of this underestimation.

Bubble growth has two stages, growth-shrinkage, and explosive growth. In the former stage, the system is in fragile equilibrium, which is actually broken up to bubble formation. The resulting critical bubble is of molecular scale under this extreme conditions. Physical properties such as surface tension, surface area, and the shape, can be very different from what are expected with macroscopic bubbles. It is difficult even with simulations to investigate them in detail, but the evaluation is important to develop a molecular theory of bubble formation.

RDFs of various states are almost the same, but the isothermal compressibility κ_T has a clear density dependence. Approaching the spinodal, κ_T increases. The kinetic instability with finite κ_T is reached before the thermodynamic instability $\kappa_T \to \infty$, but accurate calculation from simulation data is difficult due to the finite system size.

2.5 LIST OF SYMBOLS

$g(r)$	=	radial distribution function
m	=	molecular mass
k_B	=	Boltzmann constant
P	=	pressure
P_v	=	vapor pressure
P_l	=	pressure on external liquid phase
T	=	temperature
V	=	volume of the simulation cell
v	=	molecular volume
γ	=	surface tension
$\Delta n(r)$	=	residual function, defined in eq.2.5
ρ	=	total number density
ρ_l	=	number density of liquid phase

Chapter 3

BINARY LIQUIDS –DEGASSING–

3.1 Introduction

In the previous chapter, I investigated the homogeneous nucleation of the bubble in the unary liquids. In many practical situations, however, liquids contain other species. In this chapter, I investigate bubble formation in binary liquids.

Binary liquid can be categorized into two types: (1) liquid-liquid mixture such as aqueous solution of alcohol, and (2) liquid-gas mixture such as carbonated water. While solute of former system is nonvolatile, that of latter is volatile. The mechanism of bubble formation in the former case is expected to be essentially the same as that in unary system. I will focused on the latter case, i.e., liquid with dissolved gas.

Take a champagne for an example. Carbon dioxide (CO_2) gas is dissolved in aqueous solution at high pressure. When we open the bottle, the pressure is

instantly reduced to the atmospheric pressure, and the CO_2 solution becomes a supersaturated state. Generated bubbles are expected to mostly consists of CO_2. This is a typical degassing process. Since this phase change is accompanied with mass transfer in liquid, the rate of this process can be slower than the cavitation process in unary systems. Considering that the critical temperature of CO_2 is about 304 K, the CO_2 is very volatile under normal conditions.

A more extreme case is extrusion of magma. Magma deep under the ground contains much gaseous substances such as water and CO_2. When it gashes out, the dissolved gas forms bubbles, which are seen in porous lava. In this case, the temperature is much higher than the critical temperature of these gases, and the gases in bubbles are at a supercritical state.

With these examples in mind, I executed the simulation to investigate the molecular mechanism of bubble formation/growth dynamics in a liquid-gas system.

3.2 Simulation Method

I have carried out molecular dynamics simulations of a binary mixture of Lennard-Jones liquids. The system consists of 960 solute molecules(B) and 10,016 solvent molecules(A). The total number of molecules is same as the unary liquids($N_{tot} = 10,976$). These molecules interact each other via the Lennard-Jones potential,

$$\phi_{ij}(r) = 4\epsilon_{ij}\left[\left(\frac{\sigma_{ij}}{r}\right)^{12} - \left(\frac{\sigma_{ij}}{r}\right)^{6}\right] \tag{3.1}$$

$$i, j = A, B \tag{3.2}$$

with Lorentz-Berthelot mixing rules,

$$\epsilon_{AB} = \sqrt{\epsilon_{AA}\epsilon_{BB}} \tag{3.3}$$

$$\sigma_{AB} = \frac{\sigma_{AA} + \sigma_{BB}}{2}. \tag{3.4}$$

I performed our calculation with reduced units of solvent, i.e., length in σ_{AA}, energy ϵ_{AA}, and mass m_A, with the model parameters as,

$$\sigma_{AA} = \sigma_{BB},$$

$$m_A = m_B.$$

The relevant parameter of this system is the ratio of ϵ_{BB} to ϵ_{AA}. I examined two cases: (1) $\epsilon_{BB} = 0.5 \cdot \epsilon_{AA}$, and (2) $\epsilon_{BB} = 0.1 \cdot \epsilon_{AA}$. In the case of (1) I found that the mechanism of bubble formation is essentially the same as

the unary case; the bubble growth is rapid after some waiting time of bubble formation. Thus I do not discuss it further and concentrate on the case (2).

Simulations were performed at $T \sim 0.8$, which was in supercritical region for the pure solute(B-species), while subcritical region for the pure solvent(A-species). The critical temperature of pure fluid of each species are $T = 1.35$ and $T = 0.135$, respectively. At this temperature, the pure B-species does not undergo fluid phase change. Hence, we regard the solute molecules as molecules of dissolved gas in the liquid. Thus the model is supposed to be a liquid containing dissolved gas.

The method to make metastable states is similar to the previous chapter. I first prepared an equilibrium state of liquid (P in figure **??**), then expanded the equilibrated configuration of molecules uniformly and instantaneously(Q in figure 3.1). After this expansion, I continue microcanonical MD simulation with the configuration as an initial condition.

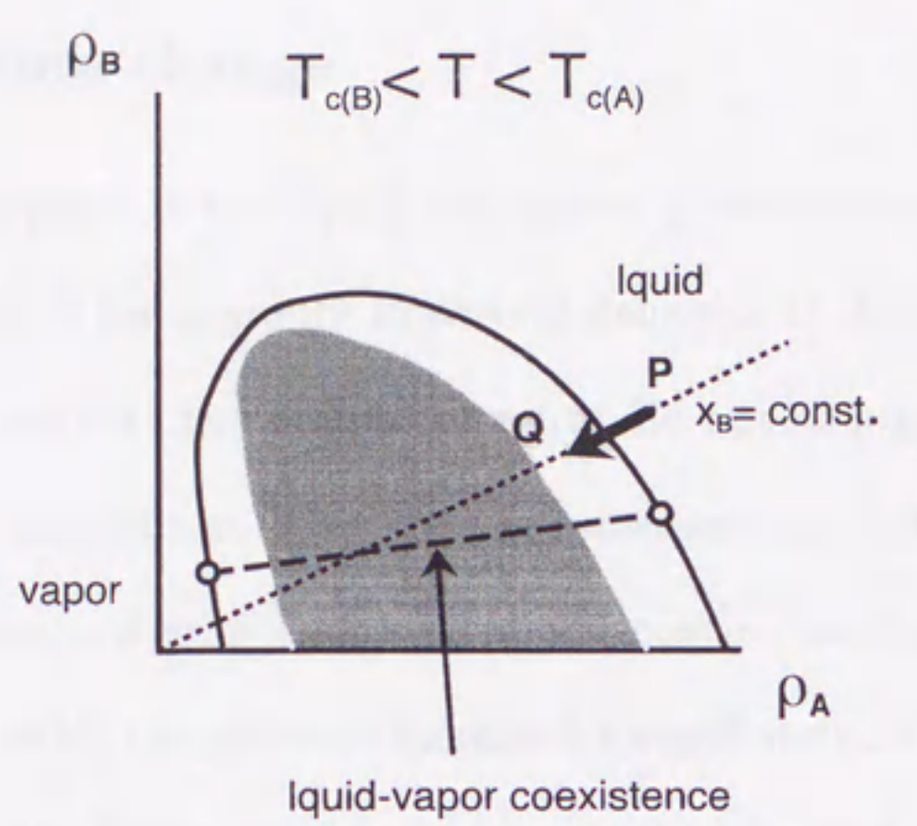

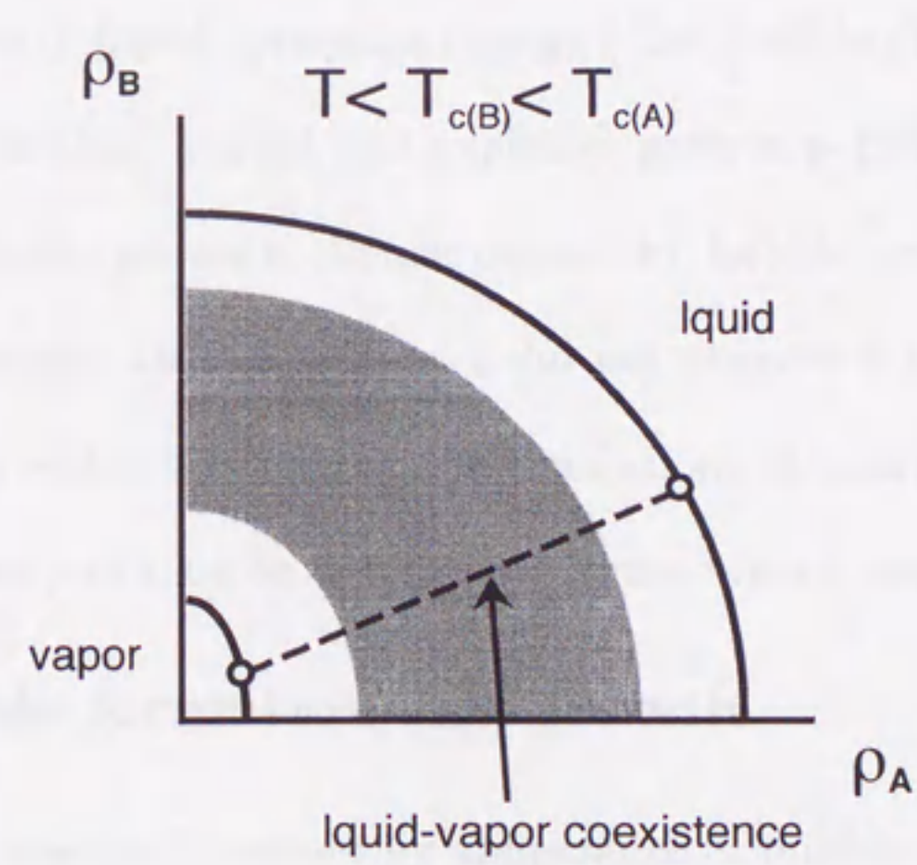

Figure 3.1: The schematic picture of phase diagram of binary liquid. This simulation is correspond to the case of $T_{c(B)} < T < T_{c(A)}$.

3.3 Results

3.3.1 Pressure change

When a bubble appears in the liquid, the system pressure must increase. The time development of the pressure in several densities is shown in figure 3.2. In the case of $\rho = 0.850$, the system pressure did not change at least in the total time of this simulation. This state is considered as stable state. In the case $\rho = 0.810$, the system pressure increased continuously. $\rho = 0.720$ is an extreme case, in which the pressure increased immediately. The results of the unary liquid and the binary liquid are compared in figure 3.3. The behavior of the pressure of the binary liquids is quite different from that of the unary liquid. In the unary liquid, pressure change (the bubble growth) has two stages; growth-shrinkage period and explosive growth period(section 2.3.3). In the binary liquid, pressure change caused by bubble growth is gradual through all the stage. In this system, I did not observe a waiting state for bubble formation which was seen in the simulations of unary liquids. Hence the limit of stability cannot be determined in the binary case.

3.3.2 Bubble formation and growth

The increase of pressure is caused by appearance of bubbles. A sequence of snapshots is shown in figure 3.4(left). These are the projection of a slice of simulation cells. A bubble appeared with the aggregation of several solute molecules ($t = 100$). The aggregation of solute molecules and the growth of

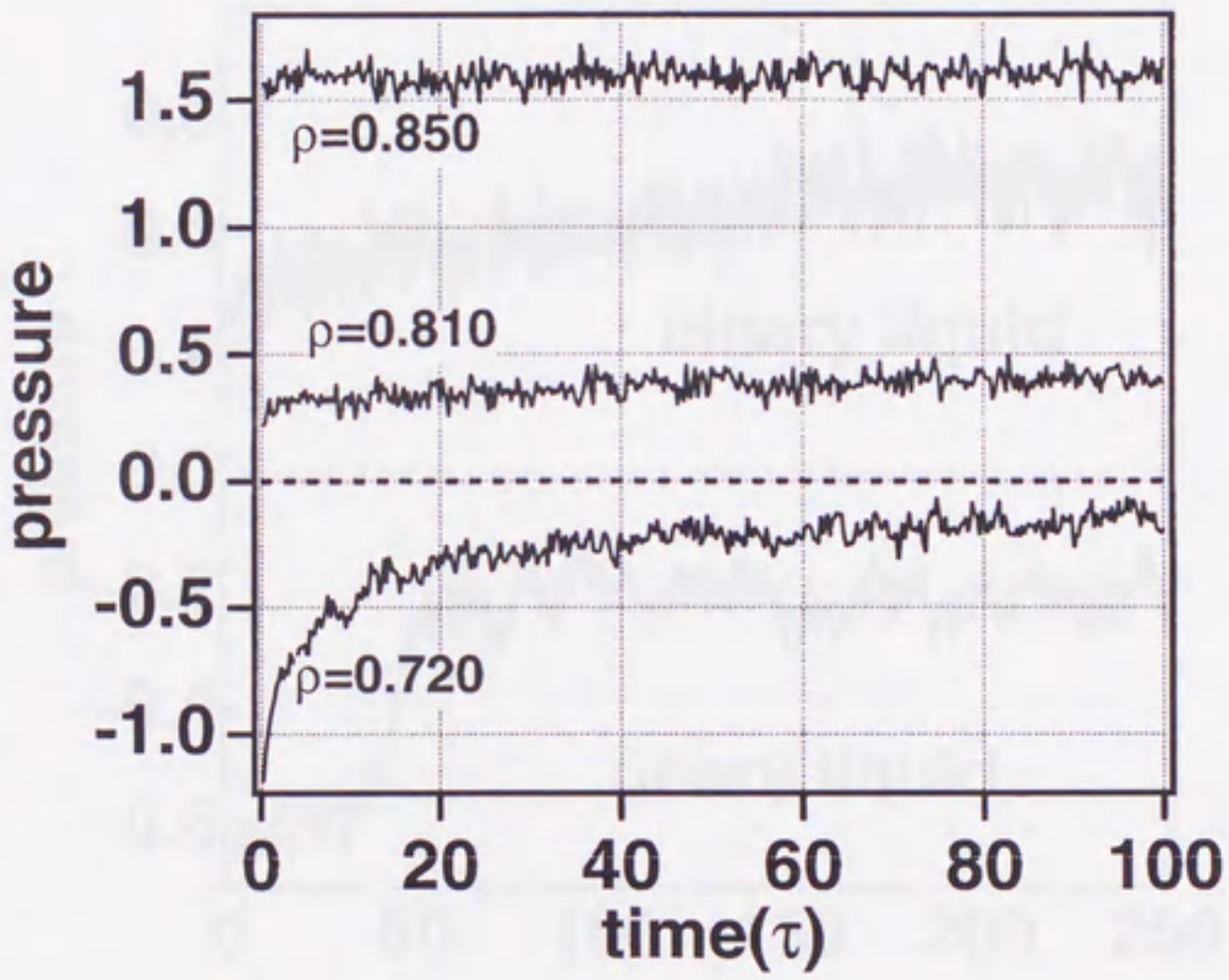

Figure 3.2: The time development of pressure.

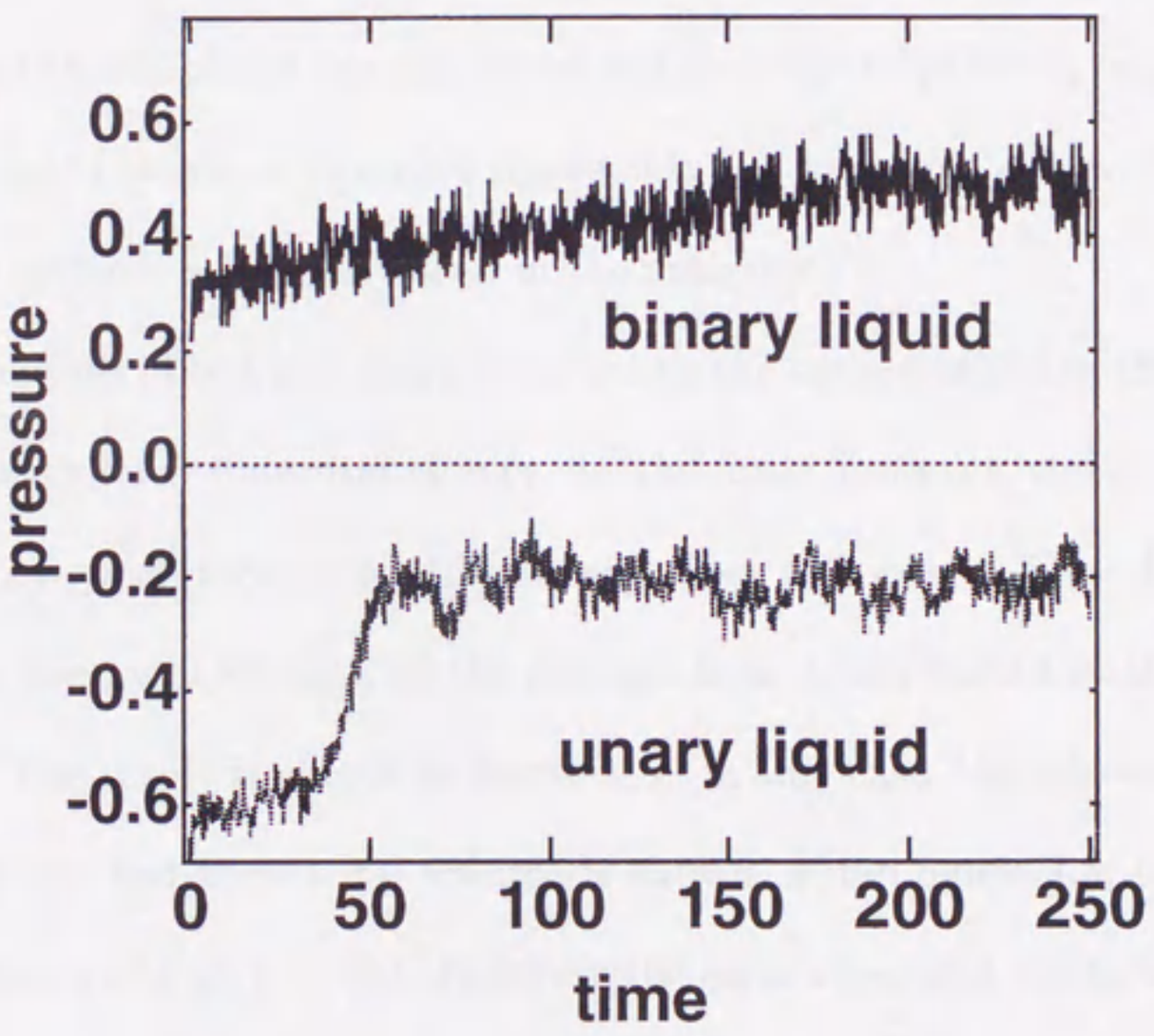

Figure 3.3: Pressure in the unary and the binary liquid.

a bubble seem to be strongly coupled.

This kind of aggregation, or fluctuations of the composition, is often seen in liquid-liquid phase transition such as alloy systems and polymer mixtures. In this system, however, the density difference between "A-rich" phase and "B-rich" phase is large because pure B can not be in a liquid state. Thus this phase separation is considered as a liquid-to-vapor transition in which A-rich phase and B-rich phase are the liquid and the vapor (bubble), respectively.

The right column of figure3.4 shows only the solute molecules. Clustering of solute molecules is clearly seen in the snapshots.

The volume of bubbles was calculated by the same method in the previous chapter with local potential energy. In this case, however, the minimum of the histogram of local potential energy does not exist. Thus I used the potential energy at plateau of the histogram as a threshold to calculate the volume. The result is shown in figure 3.5. In this case, the system contains 2—3 bubbles and their total volume is shown. From figure 3.5, the volume seems to saturate at $t \sim 200$. However the separation still continues as seen in figure 3.4.

3.3.3 Clustering of solute molecules

As shown in snapshots (figure 3.4), the growth of bubbles is associated with the aggregation of solute molecules. Hence it is expected that the bubbles are detected by investigating the clusters of solute molecules.

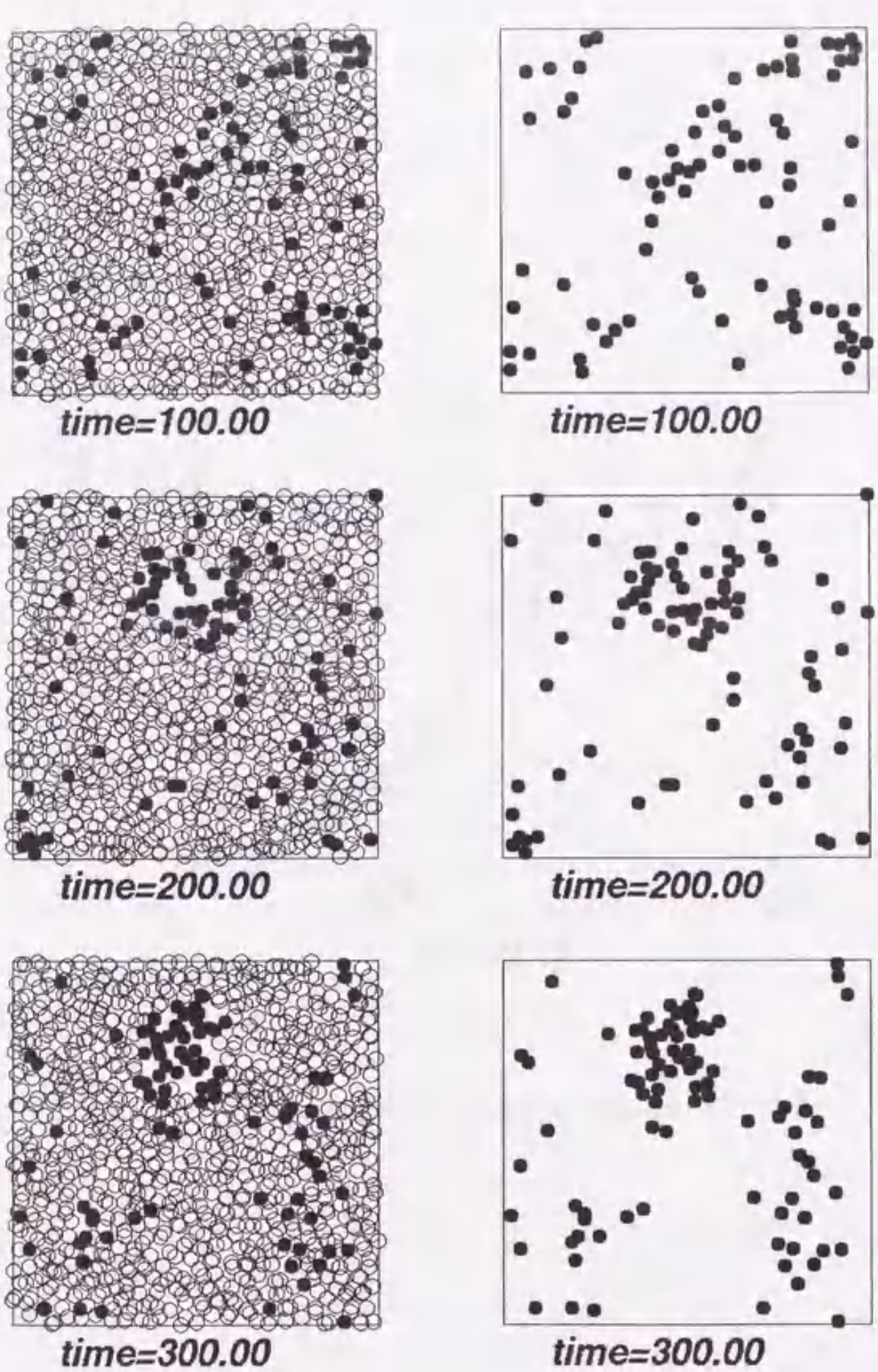

Figure 3.4: Snapshots of the binary liquid. In the right column, only solute molecules are shown.

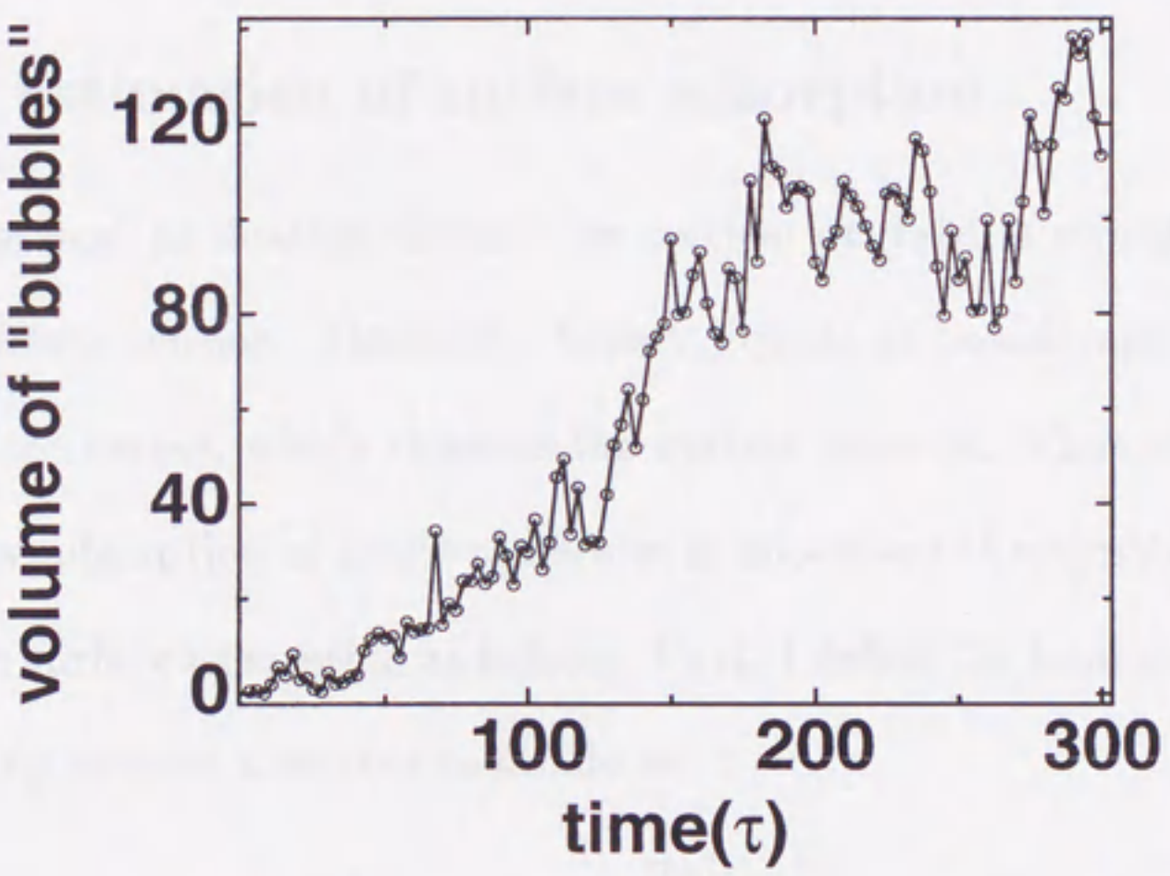

Figure 3.5: The time development of volume of bubbles

For that purpose, let us define first a connected pair of molecules as a pair the distance between which is less than $r_{\rm cut} = 1.5$. The cluster is then defined as a group of connected molecules. Figure3.6 shows the time development of size of such solute clusters. At early stage, various size of clusters existed, while at late stage, growth of two large clusters were observed. From figure 3.6, the size of the critical cluster is roughly estimated as $n^* \sim 60$. The clusters larger then n^* continues to grow.

3.3.4 Estimation of surface adsorption

In the classical nucleation theory, the nucleation rate is strongly affected by the surface tension. Generally, binary liquids at liquid-vapor interfaces have surface excess, which changes the surface tension. Thus, to calculate the surface adsorption of solute molecules is important. I estimated the total amount of surface adsorption as follows. First, I define the local mole fraction of solute x_B around a solvent molecule as

$$x_B(n) = \frac{n_B(r_{\rm cut})}{n_A(r_{\rm cut}) + n_B(r_{\rm cut})} \tag{3.5}$$

$$n = n_A(r_{\rm cut}) + n_B(r_{\rm cut})$$

where $n_A(r_{\rm cut})$ and $n_B(r_{\rm cut})$ are the number of neighboring A(solvent)-molecules and B(solute)-molecules around an A-molecule, respectively; a schematic picture is shown in figure 3.7. Figure 3.8 shows the time development of the local mole fraction. Near the surface($n \sim 6$), x_B has a sharp peak. This

is caused by surface adsorption, hence we can estimate the total amount of surface adsorption as

$$n_s = \sum_{\text{surface}} f_{\text{n}}(n)(x_B(n) - \overline{x_B}) \tag{3.6}$$

where $\overline{x_B}$ is the total mole fraction. In the summation, we take the surface region as $5 \leq n \leq 8$. Figure 3.9 shows the time development of the surface adsorption. Though it increases almost monotonously, there seems to be a drop at $t = 300$. As indicated in figure 3.4, this may be caused by evaporation of solute molecules which were adsorbed on the bubble surface .

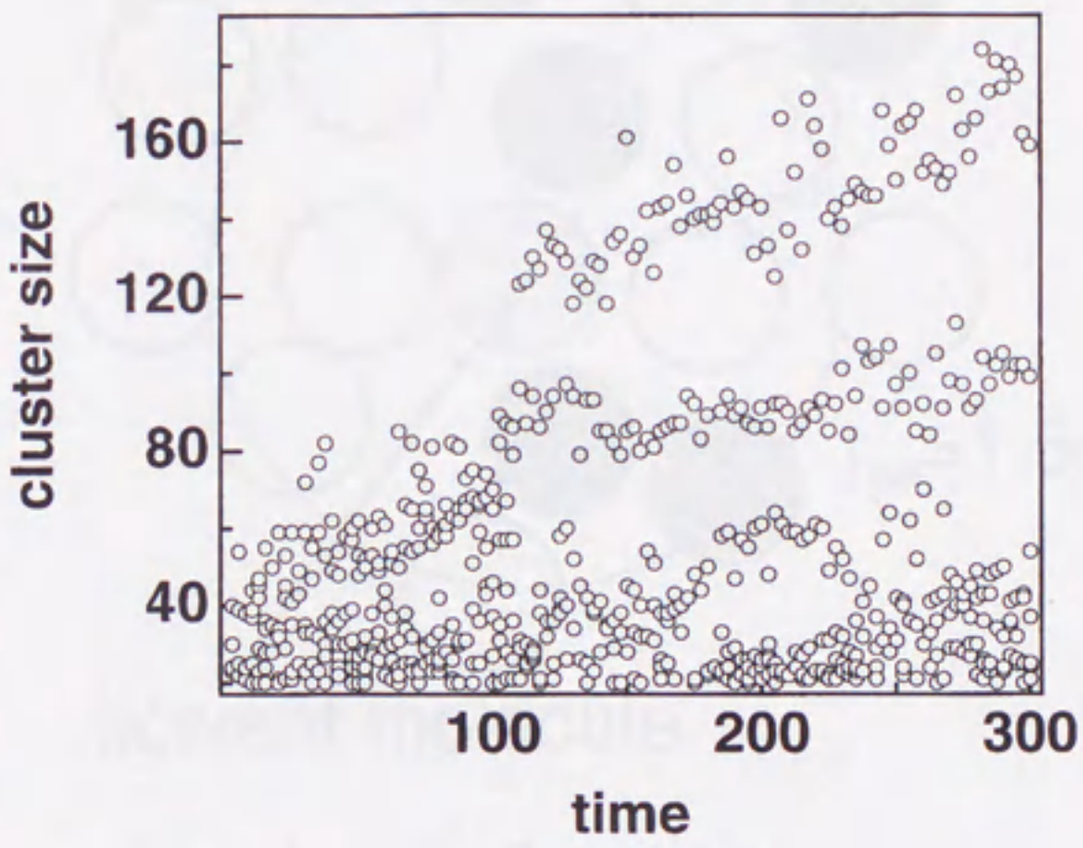

Figure 3.6: The time development of cluster size.

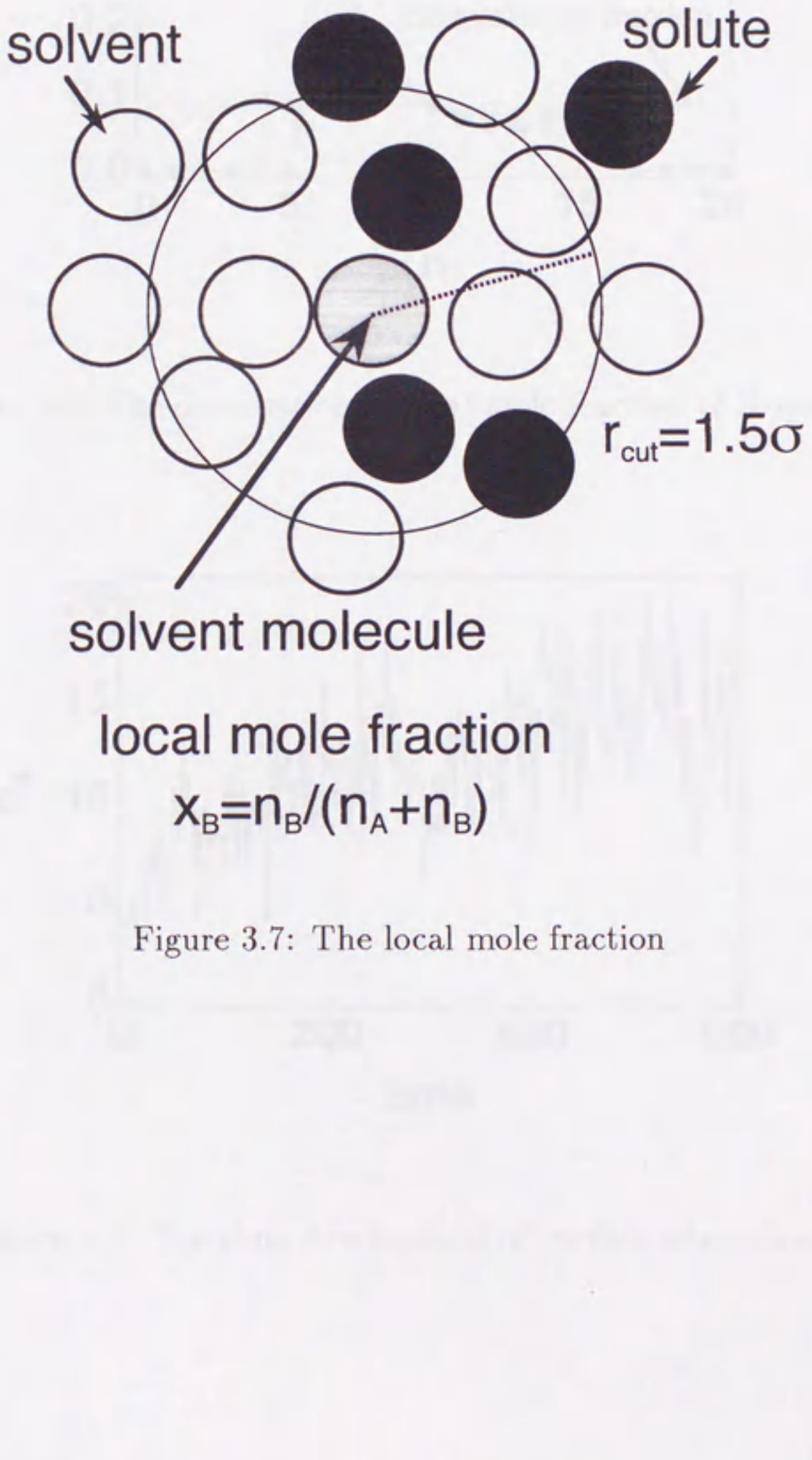

Figure 3.7: The local mole fraction

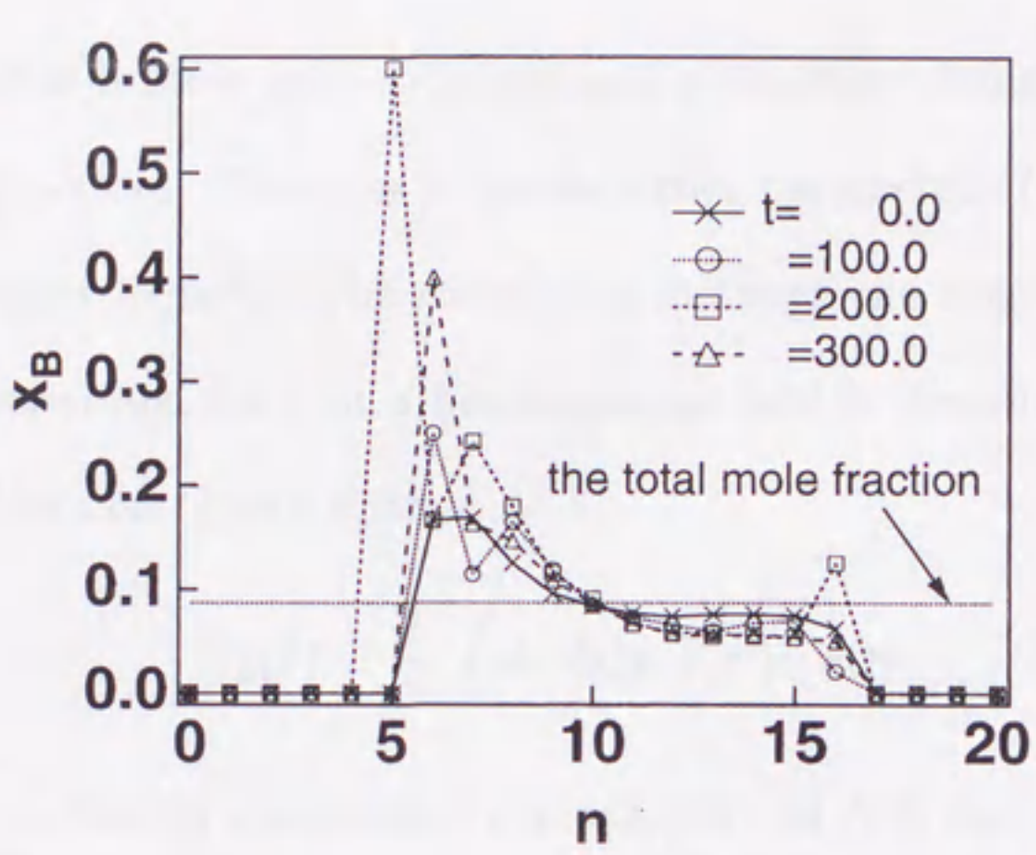

Figure 3.8: The distribution of local mole fraction of B-species

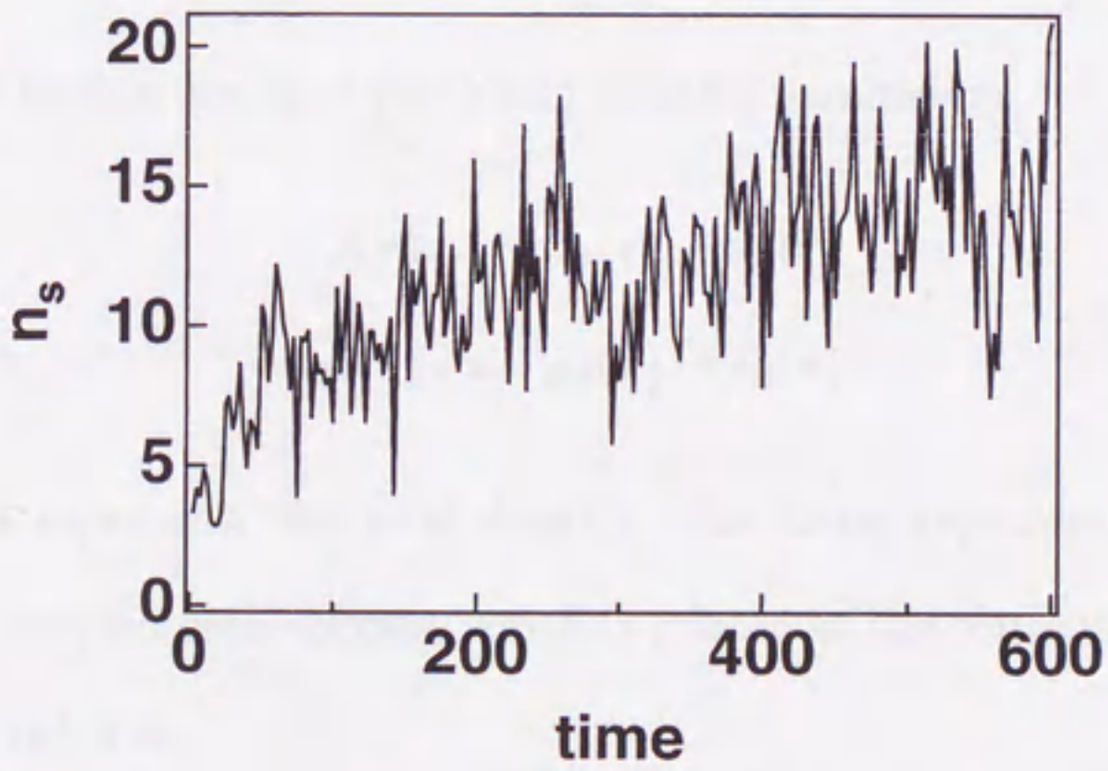

Figure 3.9: The time development of surface adsorption.

3.3.5 Time development of structure factor

Structure factor is often used to investigate a structure change during phase separation processes. Consider a spatial order parameter $a(\boldsymbol{r})$ corresponding to a number density. The correlation between the order parameter at two points separated by $\boldsymbol{r}$ in a homogeneous fluid is described by an auto correlation function $G_a(\boldsymbol{r})$, defined as

$$G_a(\boldsymbol{r}) = \frac{1}{N}\int d\boldsymbol{r}' \langle a(\boldsymbol{r}+\boldsymbol{r}')a(\boldsymbol{r}')\rangle \tag{3.7}$$

where $< \cdots >$ denotes a statistical average [30] and N is the total number of particles. The static structure factor $S_a(\boldsymbol{k})$ is defined as a Fourier transform,

$$\begin{aligned} S_a(\boldsymbol{k}) &= \int d\boldsymbol{r} G_a(\boldsymbol{r}) \exp\Big[-i\boldsymbol{k}\cdot\boldsymbol{r}\Big] & (3.8)\\ &= \frac{1}{N}\int d\boldsymbol{r} d\boldsymbol{r}' \langle a(\boldsymbol{r}+\boldsymbol{r})a(\boldsymbol{r}')\rangle \exp\Big[-i\boldsymbol{k}\cdot\boldsymbol{r}\Big]. & (3.9)\end{aligned}$$

For binary liquids, we have two kinds of order parameters,

$$\begin{aligned} \rho(\boldsymbol{r}) &= \rho_A(\boldsymbol{r}) + \rho_B(\boldsymbol{r}) & (3.10)\\ \psi(\boldsymbol{r}) &= \rho_A(\boldsymbol{r}) - \rho_B(\boldsymbol{r}) & (3.11)\end{aligned}$$

The former represents the total density. The latter represents the density difference between each species, which is related to the composition of B(or A) species $c_{\mathrm{B}}(\boldsymbol{r})$ as,

$$\psi = (2c_{\mathrm{B}} - 1)\rho. \tag{3.12}$$

Thus $\psi(\boldsymbol{r})$ is suitable to describe liquid-liquid phase separations.

Microscopically, the local density of each species is defined with the position of i-th particle $\boldsymbol{r}_i^X$ of species X (X=A or B) as

$$\rho_A(\boldsymbol{r}) \equiv \sum_{n=1}^{N_A} \delta(\boldsymbol{r} - \boldsymbol{r}_n^A), \tag{3.13}$$

$$\rho_B(\boldsymbol{r}) \equiv \sum_{n=1}^{N_B} \delta(\boldsymbol{r} - \boldsymbol{r}_n^B). \tag{3.14}$$

The structure factors are then written as

$$S_{A+B}(\boldsymbol{k}) = \langle [\rho_A(\boldsymbol{k}) + \rho_B(\boldsymbol{k})] [\rho_A(-\boldsymbol{k}) + \rho_B(-\boldsymbol{k})] \rangle \tag{3.15}$$

$$S_{A-B}(\boldsymbol{k}) = \langle [\rho_A(\boldsymbol{k}) - \rho_B(\boldsymbol{k})] [\rho_A(-\boldsymbol{k}) - \rho_B(-\boldsymbol{k})] \rangle \tag{3.16}$$

where

$$\rho_X(\boldsymbol{k}) = \sum_{n=1}^{N_X} \exp(-i\boldsymbol{k} \cdot \boldsymbol{r}_n^X) \quad X = A \quad \text{or} \quad B \tag{3.17}$$

are the Fourier transform of the local densities.

$S_{A+B}(\boldsymbol{k})$ and $S_{A-B}(\boldsymbol{k})$ describe the structure of the density fluctuations and the composition fluctuations, respectively. I calculated these two structure factors to investigate the coupling of liquid-liquid phase separation and liquid-vapor separation. The time developments of $S_{A+B}(k)$ and $S_{A-B}(k)$ are shown in figures 3.10 and 3.11. In both of the structure factors a sharp peak rises at the wave number $k_{\max} \sim 0.5$. The heights of these peaks increase simultaneously. This means density fluctuations and composition fluctuations grow up together. The wave number at the peak roughly describes the characteristic length scale as, $\lambda = 2\pi/k_{\max}$. In this case the characteristic length

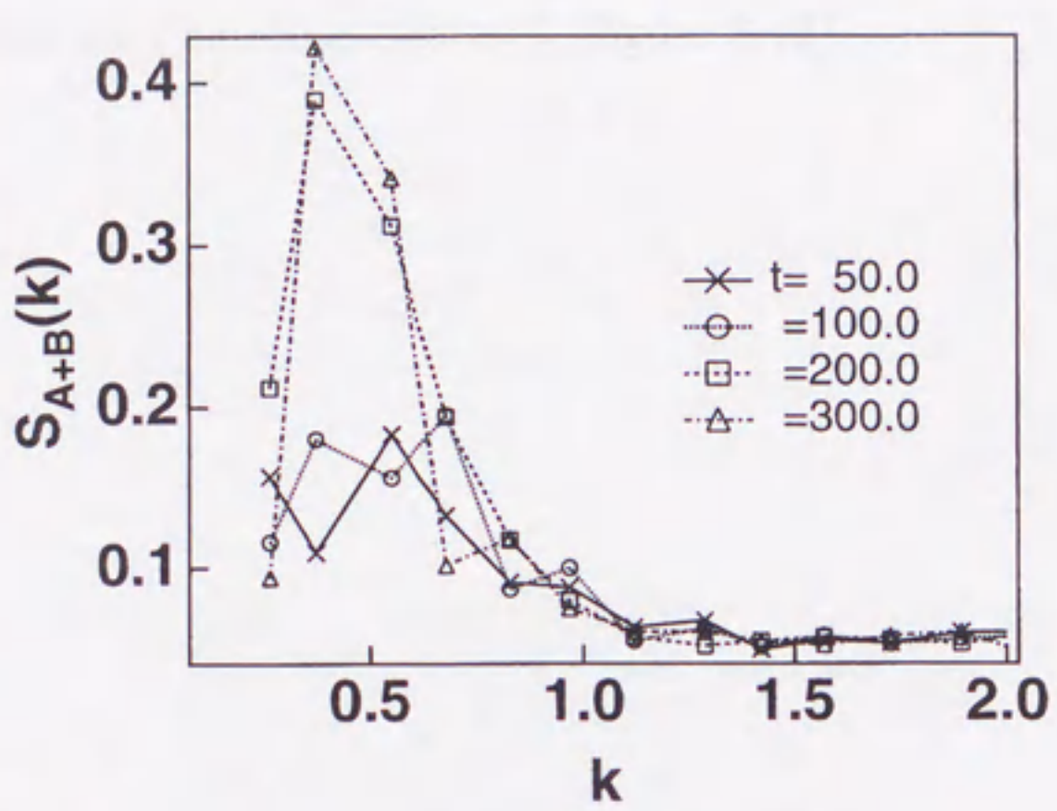

Figure 3.10: Structure factor $S_{A+B}(k)$

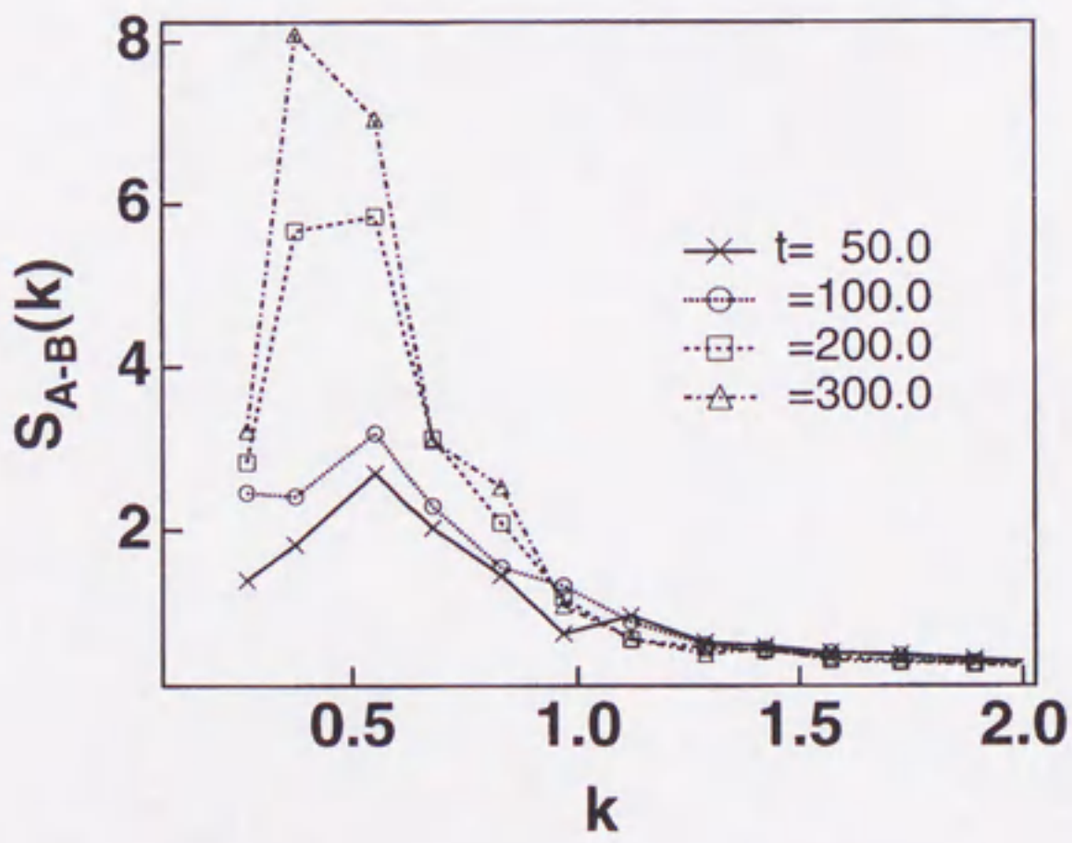

Figure 3.11: Structure factor $S_{A-B}(k)$

is estimated as $\lambda \sim 12$. In the binary liquid several bubbles were observed. These bubbles may be separated by λ (figure 3.12).

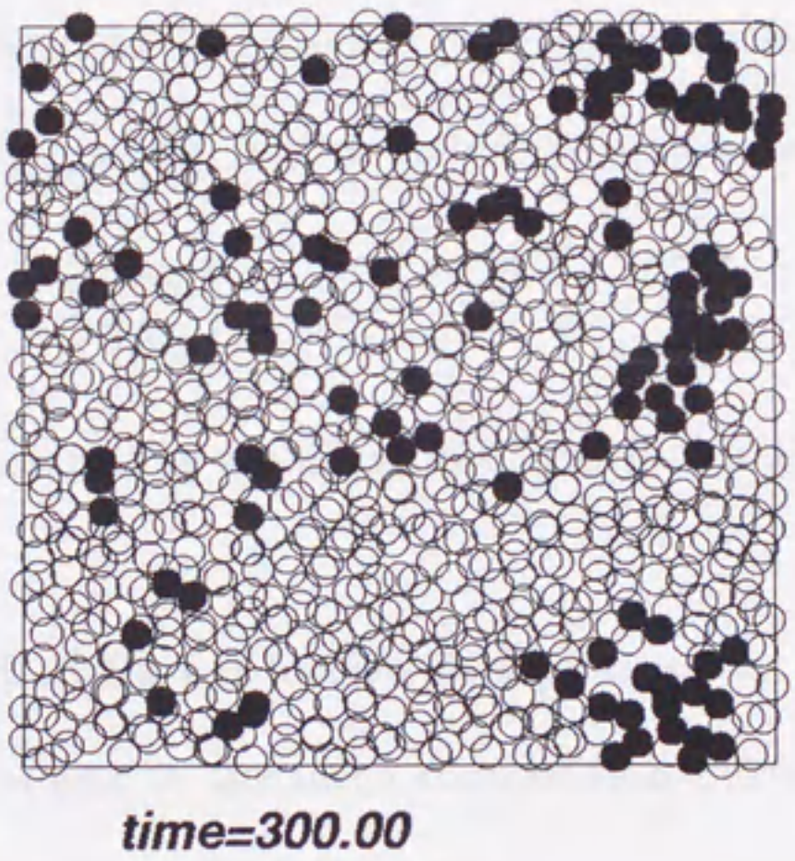

Figure 3.12: The peak of the structure factor $S_{A\pm B}(k)$ corresponds to the characteristic length. The length of unit cubic cell is about 24.

3.4 Discussion

In this chapter, I investigated the degassing process. The mechanism of bubble formation is different from the unary case. The pressure change associated with the bubble formation was gradual. This is caused by the strong coupling between liquid-liquid phase separation and liquid-vapor separation.

It is known that the thermodynamic stability of a binary system is first violated by fluctuations of composition [6]. The condition of the thermodynamic limit of stability of the binary system is written as

$$\left(\frac{\partial \mu_{_B}}{\partial N_{_B}}\right)_{T,\mu_A,V} = \frac{k_{\mathrm{B}}T}{\langle (\delta N_{_B})^2 \rangle_{_V}} = 0. \tag{3.18}$$

Thus, when approaching the stability limit, the fluctuations of composition should diverge.

In our system, bubbles are formed and grow up by clustering of solute molecules, corresponding to the large composition fluctuations. I observed two clusters growing, from which the critical size of bubbles is estimated as a cluster of solute molecules. The variation of static structure factor also shows the coupling of the above two kinds of phase separation, liquid-liquid (composition fluctuations) and liquid-vapor (density fluctuations).

The total surface adsorption was estimated. The time development of the surface adsorption exhibits a drop at $t = 300$. This implies the evaporation of solute molecules which were adsorbed on the bubble surface.

3.5 LIST OF SYMBOLS

k_B = Boltzmann constant
T = temperature in unit of ϵ_{AA}/k_B
P = pressure in unit of $\epsilon_{AA}/\sigma_{AA}^3$
m_i = molecular mass
σ_{ij} = diameter of molecule
ϵ_{ij} = depth of potential of molecule
τ = unit of time ($= \sqrt{m_A \sigma_{AA}^2/\epsilon_{AA}}$)

Chapter 4

CONCLUSION

In this thesis, I have investigated bubble formation in liquids using large scale molecular dynamics simulations. Bubble formations in unary and binary liquids occur by essentially different mechanism. While in the unary liquids, density fluctuations initiate bubble formation, in binary liquids(liquids with dissolved gas), composition fluctuations initiate it. The growth process of bubbles in these two systems are also different; explosive growth in the unary liquid and gradual growth in the binary liquid. The latter is dominated by diffusion process of solute molecules in the solvent liquid. The results are summarized in following,

The unary liquid

1. The stability limits of liquid are obtained.

2. The size of the bubble defined by (2.4) increases rapidly after several cycle of growth-shrinkage around $r \sim 1$. This radius corresponds to the critical radius.

3. The nucleation rate is calculated from the waiting time (τ_{w}) for bubble formation. The calculated nucleation rate is 17 orders of magnitude lager than prediction of classical nucleation theory. This under estimation of rate in classical nucleation theory is caused by the residue of free energy barrier even at spinodal.

4. In the simulations, the height of free energy barrier to form a critical bubble is overcome by thermal fluctuations which is roughly estimated as $W^*_{\mathrm{min}} \sim k_{\mathrm{B}}T$. On the other hand, the predicted value is $W^*_{\mathrm{min}} \sim 50$ which is unlikely overcome by fluctuations. The size (radius) of the critical bubble is ~ 1 for simulations, compared with ~ 3 for prediction.

The binary liquid

1. As opposed to the unary liquid, the growth of bubble is gradual through all the stage. The rate of growth is considered to be determined by the diffusion rate of solute molecules .

2. Bubble formation and growth are associated with clustering of solute molecules. The critical size of a bubble as a cluster of solute molecules is roughly estimated as $n^* \sim 60$.

3. The local mole fractions have a sharp peak near the surface ($n \sim 6$) from which surface adsorption is estimated.

4. The total surface adsorption is evaluated by definition (3.6). There seems to exhibit a drop at $t = 300$. This may be caused by evaporation of solute molecules which were adsorbed in bubble surface (see fig3.4).

5. The peak of structure factors $S_{A+B}(k)$ and $S_{A-B}(k)$ are simultaneously increase. This means the density fluctuation and composition fluctuation grow up concurrently.

6. The state of pure liquid corresponding to the binary mixture in terms of its number density is very close to the coexistence curve. Thus free energy barrier of pure liquid is extremely high ($W^*_{\min} \sim 1500$) and the size of the critical nucleus is ~ 20; spontaneous bubble formation never occur in the unary liquid at this condition. Dissolved gas drastically reduces the barrier to $\sim k_B T$ and the size to ~ 5, by composition fluctuations.

In this work, I have developed various methods to execute the MD simulation in an efficient way, evaluate the system properties quantitatively, and investigate microscopic dynamics in details. I applied them to simple fluid systems which are the fundamentals to understand the bubble formation mechanism, and proved the usefulness of these methods.

In many fields of science and engineering, these bubble formation behaviors are widely seen for various substances, such as associating fluids (eg.,

water and alcohols), electrolyte solutions, and molten salts (eg., magma and lava flow). Their molecular interactions are much more complex than the simple fluid I studied here, but I believe that similar methods are still applicable. In this sense, this work is our first step to study the fluid phase transition at molecular level.

Bibliography

[1] D. H. Trevena. *Cavitation and Tension in Liquids.* Adam Hilger, Bristol, 1987.

[2] J. D. Gunton, M. S. Miguel, and P. S. Sahni. The dynamics of first-order phase transitions. In C. Domb and J. Lebowitz, editors, *Phase Transistion*, Vol. 8. Academic Press, London, 1983.

[3] K Binder. Mechanisms for the dynamics of phase transformation. In *Lecture Notes for NATO ARW "Condensed Matter Resarch Using Nutrons, Today and Tomorrow"*. Plenum press, 1984.

[4] J. P. Hirth and G. M. Pound. *Condensation and Evaporation.* Pergamon Press, 1963. Chapter F Ebullition and Cavitation in Liquids.

[5] M. P. Allen. *Computer Simulation of Liquids.* Oxford University Press, Oxford, 1987.

[6] P. G. Debenedetti. *Metastable Liquids: Concepts and Prinsiple.* Prinston Univ. Press, Prinston, 1996.

[7] R. Becher and W. Döring. Kinetische behandlung der keimbildurng in übersättigten dampfen. *Ann. Phys.*, Vol. 24, p. 719, 1935.

[8] D. W. Oxtoby. Nonclassical nucleation: Theory and experiment. *J. Phys.: Condens. Matter.*, Vol. 4, pp. 7627–7650, 1992.

[9] M. Blander and J. L. Katz. Bubble nucleation in liquids. *AIChE J.*, Vol. 21, pp. 833–848, 1975.

[10] A. Laaksonen, V. Talanquer, and D. W. Oxtoby. Nucleation: Measurements, theory and atmospheric applications. *Annu. Rev. Phys. Chem.*, Vol. 46, pp. 489–524, 1995.

[11] R. H. Heist and H. He. Review of vapor to liquid homogeneous nucleation experiments from 1986 to 1992. *J. Phys. Chem. Ref. Data*, Vol. 23, pp. 781–805, 1994.

[12] R. Strey, P. E. Wagner, and Y. Viisanen. The problem of measuring homogeneous nucleation rate and the molecular contents of nuclei: Progress in the form of nucleation pulse measurements. *J. Chem.Phys.*, Vol. 98, pp. 7748–7758, 1994.

[13] C. T. Avedisian. The homogenious nucleation limits of liquids. *J. Phys. Chem. Ref. Data*, Vol. 14, pp. 695–729, 1985.

[14] V. P. Skripov and athers. *Thermophysical Properties of Liquid in the Metastable State.* Gordon and Breach Science Publishers, New York, 1988.

[15] Y. Ohde and athers. The two-stage increase in negative pressure with repeated cavitation for water in a metal Bertherot tube. *J. Phys. D: Appl. Phys.*, Vol. 21, pp. 1540–1542, 1988.

[16] V. N. Chakanov. In percoration of relevance to the superheating of light and heavy water? *J. Chem. Phys.*, Vol. 83, pp. 1902–1908, 1985.

[17] V. G. Baidakov, A. M Kaverin, and G. Sh. Boltachev. Nucleation in superheated liquid argon-ktypton solution. *J. Chem. Phys.*, Vol. 106, pp. 5648–5657, 1997.

[18] Y. Iida, K. Okuyama, and K. Sakurai. boiling nucleation on a very small film heater subjected to extremly rapid heating. *Int. J. Heat Mass Transfer..*, Vol. 37, pp. 2771–2780, 1994.

[19] C. E. Brennen. *Cavitation and Bubble Dynamics.* Oxford University Press, 1995.

[20] J. J. Nicolas, K. E. Gubbins, W. B. Streett, and W. B. Tildesley. Equation of state for the Lennard-Jones fluid. *Mol. Phys.*, Vol. 37, pp. 1429–1454, 1979.

[21] J. P. Hirth, G. M. Pound, and G. R. St. Pierre. Bubble nucleation. *Metall. Trans.*, Vol. 1, pp. 939–945, 1970.

[22] K. Yasuoka. *Molecular Dynamics Simulation of Homogeneous Nucleation in Vapor Phase.* PhD thesis, Nagoya University, 1997.

[23] J. K. Johnson, J. A. Zollweg, and K. E. Gubbins. The Lennard-Jones equation of state revisited. *Mol. Phys.*, Vol. 78, pp. 591–618, 1993.

[24] X. C. Zeng and D. W. Oxtoby. Gas-liquid nucleation in Lennard-Jones fluids. *J. Chem. Phys.*, Vol. 94, pp. 4472–4478, 1991.

[25] D. W. Oxtoby and R. Evans. Nonclassical nucleation theory for the gas-liquid transition. *J. Chem. Phys.*, Vol. 89, pp. 7521–7530, 1988.

[26] X. C. Zeng. Gas-liquid nucleation in two-dimensional fluids. *J. Chem. Phys.*, Vol. 104, pp. 2699–2704, 1996.

[27] J. W. Cahn and J. E. Hilliard. Free energy of a nonuniform system. I. Interfacial free enaergy. *J. Chem. Phys.*, Vol. 28, pp. 258–267, 1958.

[28] J. W. Cahn. Free energy of a nonuniform system. II. Thermodynamic basis. *J. Chem. Phys.*, Vol. 30, pp. 1121–1124, 1959.

[29] J. W. Cahn and J. E. Hilliard. Free energy of a nonuniform system. III. Nucleation in a two-compornent incompressible fluid. *J. Chem. Phys.*, Vol. 31, pp. 688–699, 1959.

[30] J.-P. Hansen and I.R. McDonald. *Theory of Simple Liquids.* Academic Press, New York, 2nd edition, 1986.

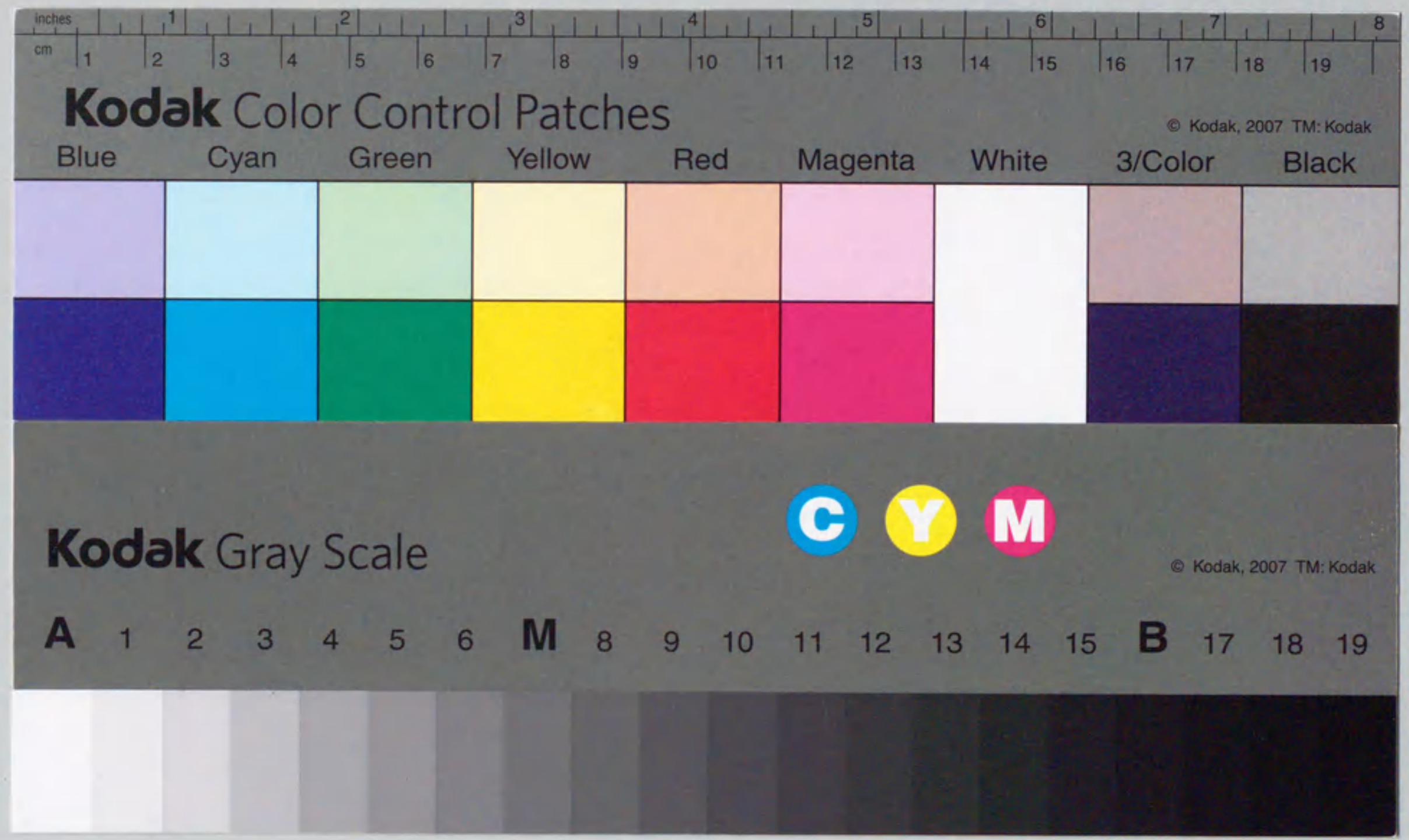
inches
cm
Kodak Color Control Patches
© Kodak, 2007 TM: Kodak
Blue
Cyan
Green
Yellow
Red
Magenta
White
3/Color
Black
Kodak Gray Scale
C
Y
M
© Kodak, 2007 TM: Kodak
A 1 2 3 4 5 6 M 8 9 10 11 12 13 14 15 B 17 18 19